IMPROVEMENT OF SIGNAL-TO-NOISE AND SELECTIVITY IN FLUORESCENCE SPECTROMETRY

BY

Gary Lyle Walden

A DISSERTATION PRESENTED TO THE GRADUATE COUNCIL OF
THE UNIVERSITY OF FLORIDA
IN PARTIAL FULFILLMENT OF THE REQUIREMENTS FOR THE
DEGREE OF DOCTOR OF PHILOSOPHY

UNIVERSITY OF FLORIDA

1979

ACKNOWLEDGEMENTS

I wish to express my graditude to my research director, Dr. James D. Winefordner, for his constant help, encouragement, and belief. Special thanks to Jim Bower and Jimmie Ward for their aid and advice. Thanks to Dave Bolton for help with the assembly language programming and to Jeanne Burton for the hours spent on this document. Also, my graditude is extended to the JDW group, past and present.

I would like to thank my parents, Raymond and Elma Walden, for their support, and finally to my wife, Marsha, for her sacrifice, patience, and devotion.

TABLE OF CONTENTS

LIST OF TABLES

LIST OF FIGURES

Figures Page

Abstract of Dissertation Presented to the Graduate Council of the University of Florida in Partial Fulfillment of the Requirements for the Degree of Doctor of Philosophy

IMPROVEMENT OF SIGNAL-TO-NOISE AND SELECTIVITY IN FLUORESCENCE SPECTROMETRY

By

Gary Lyle Walden

December 1979

Chairman: James D. Winefordner
Major Department: Chemistry

The aim of this work was to improve molecular fluorimetric analysis. Since the noise attributed to an analysis system is the limiting property of the determination, the noise spectral analysis of the system is important. The noise power spectra of an inductively coupled plasma (ICP) were determined as an example of a typical radiative source. The system used for the fluorimetric analysis was a pulsed source-gated temporal detector.

Noise power spectra for the ICP were determined under various conditions by Fast Fourier Transform (FFT) digital techniques. The quantitative results for the three major noise components are given. These noise components are white noise, low frequency noise, and proportional noise. The proportional noise observed increased with concentration of analyte, radio frequency (RF) power, nebulizer flow rate,

and coolant gas flow rate. Increasing the observation wavelength increased the frequency at which the low frequency component reached 10% of its maximum amplitude. Changing the observation height in the plasma determined which noise components were visible in the power spectrum. At observation heights near the power coils, all three noise components were present, whereas, at a significantly greater height, primarily the low frequency noise dominated. Changing the torch design changed the relative amplitudes of the different proportional noise components, but did not greatly change the central frequencies. Changing the drain tube length or cavity volume had little effect on the noise power spectra.

Also reported is the temporal measurement of fluorescence signals using two different pulse measurement techniques. The first measurement technique discussed is a photomultiplier tube-boxcar (PM-boxcar) approach. The second is a streak camera system. Although the PM-boxcar system was more sensitive, it suffered from poor overall temporal resolution due to trigger jitter and PM temporal response. The streak camera approach is by far the best in terms of temporal resolution, however, the signal levels needed for its operation are quite large. The streak camera was used to determine external heavy atom effects on fluorescence lifetimes and an attempt was made to recover the fluorescence lifetimes of two spectrally overlapping compounds in a mixture. A comparison of the most often used temporal measurement techniques for fluorescence is given.

CHAPTER I
BACKGROUND INTRODUCTION

When molecular luminescence is used for analysis, the analyst must be aware of the overall signal-to-noise ratio (S/N) of the method. Whenever he attempts to improve a method, he is trying to increase the signal and/or lower the effective noise in order to increase S/N. Through the use of theoretical S/N consideration, described by Alkemade et al. (1), Boutilier et al. (2,3), and Boutilier (4), it is possible to determine certain experimental approaches which could lead to an increase in the S/N. However, this must be done only with the inclusion of previous experimental knowledge and must be tested under actual experimental conditions. To quote I.M. Kolthoff, "Theory guides, experiment decides."

The effect of the S/N on analytical figures of merit are important to visualize. The limit of detection (LOD) is the most obvious case in which an improvement in S/N results in a lower LOD. Using the IUPAC definition (5), the limit of detection is the analyte concentration, or amount, that corresponds to a measure (signal) equal to three times the standard deviation ("noise") of the measurement of the blank for a sufficiently large number of blank determinations (16 suggested). More simply, the concentration that results in a S/N of three.

Another figure of merit affected is the linear dynamic range (LDR). An increase in the S/N generally results in an increase of the LDR, barring any other change in the analytical calibration curve, and hence, increases the useful working range of the method. Also by increasing the S/N, the percent relative standard deviation (%RSD) decreases, which is an improvement in the precision of the method.

Noise Power Spectra

As implied from the definition of limit of detection, if a signal is present, from a given system, the S/N can be improved simply by decreasing the noise component to its absolute minimum (assuming that point has not already been reached). The determination of the noise components in a given system and their contribution to the overall noise of the method is of paramount importance in improving any method. The determination of the noise components in a system is experimentally accomplished by obtaining the noise power spectra for that system. Classically, this has been done in a rather laborious fashion (6-8). With the advent of modern computers and the development of the Fast Fourier Transform (FFT) (9-11), this process has been simplified (12). At the present, there are several commercially available FFT instruments. With either method, the information obtained is a power measurement per frequency interval (units proportional to W Hz^{-1}) over a given frequency range. As will be

discussed later, this information can be used to define analytical working conditions or even to localize and eliminate or minimize noise sources. It is also possible to use these measurements to decide upon experimental setups where signal power might be greater at certain frequencies and/or where noise power is lower.

As an application of the determination of noise power spectra, the present work is applied to a popular atomic emission source, an inductively coupled argon plasma (ICP). The noise power spectra obtained indicate the possible application of an AC detection system. The use of noise power as a diagnostic tool for torch design and characterization is also indicated.

Previous workers (6-13) have described the power spectra of several sources of analytical importance. In most cases, the noise power spectra are composed of a low frequency, assumed to be of the 1/f variety, component of considerable amplitude, proportional noise, spikes due to the 60 cycle line frequency and its harmonics, and a white noise background that extends throughout the spectra. Also reported in certain cases are higher frequency proportional noise components, so called whistle noise (1). In the present work, all of these noise types were observed in the ICP under various conditions. Different experimental parameters were changed and the effects noted.

Fluorescence Theoretical Background

In molecular luminescence spectrometry, the noise sources are a subset of the type of measurement approach chosen. In the present work, molecular fluorimetry is the technique used.

Fluorescence of an organic molecule corresponds to the radiative transition of an excited molecule from its excited state singlet, S_1, to the singlet ground state, S_0 (refer to Figure 1). If the molecular population of a single species is instantaneously displaced from equilibrium, e.g., by a burst of excitation light, the population will decay back to equilibrium by emitting fluorescence radiation that will follow an exponential function given by

$$I = I_0 e^{-t/\tau_F} \qquad (1)$$

where t is time, I is the observed fluorescence intensity, I_0 is the fluorescence intensity at time t = 0 (where t = 0 is some time after the burst of excitation light has ended), and τ_F is the observed lifetime of the fluorescence. The observed fluorescence lifetime is determined to be the time it takes the intensity of the fluorescence to decay to 1/e of its value at t = 0. Hence, the observed lifetime is the reciprocal of the rate at which the excited population decays back to equilibrium. This rate is determined by a combination of rate constants of the different processes that are occurring in the excited state molecular population (see

Figure 1. Energy Level Diagram

k = rate constant

A = Absorption
F = Fluorescence
P = Phosphorescence
IC = Internal conversion (radiationless transition between states of equal spin)
ISC = Intersystem crossing (radiationless transition between spin forbidden states)
ISC^* = $T_1 \rightarrow S_0$ (radiationless transition)
S_0 = Singlet ground state
S_1 = Excited singlet state
T_1 = Excited triplet state

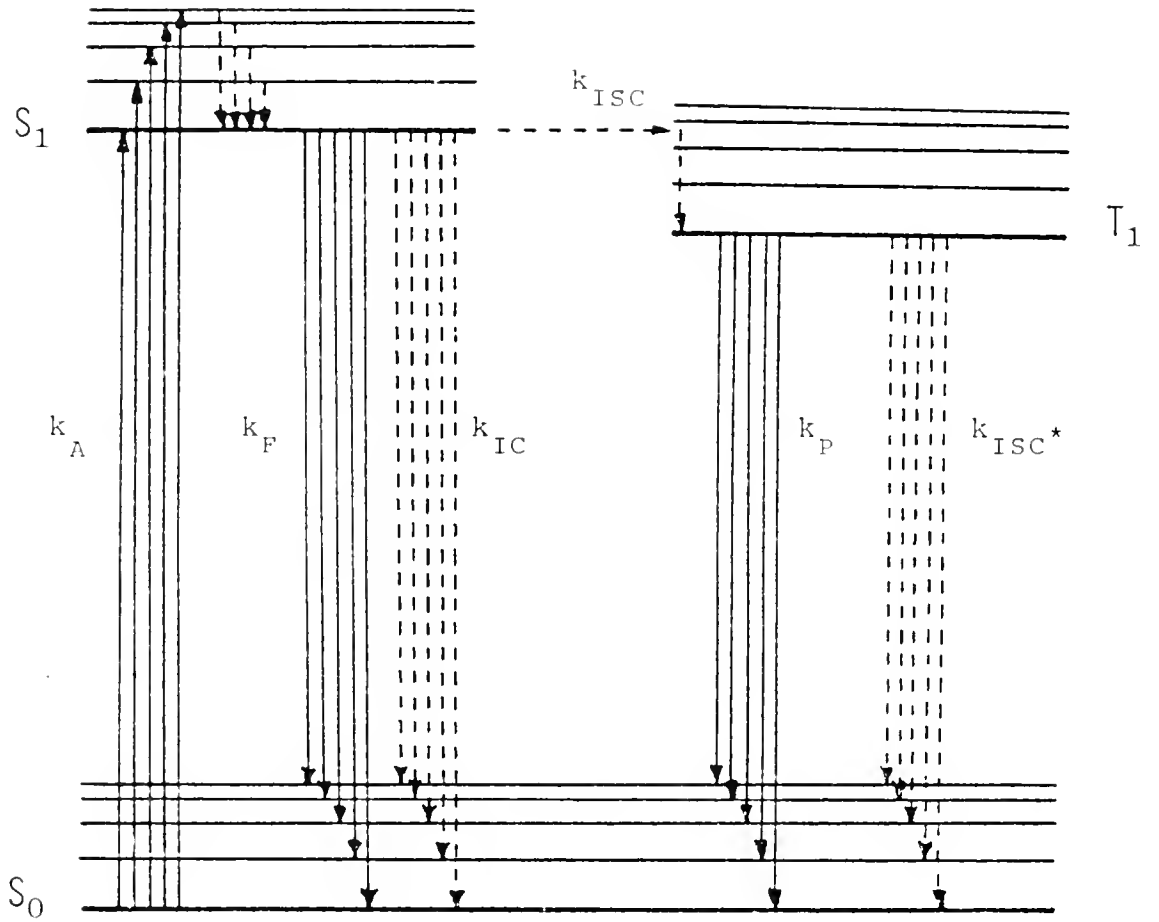
S_1
k_{ISC}
T_1
k_A
k_F
k_{IC}
k_P
$k_{ISC}*$
S_0

Figure 1). There are three main processes contributing to the decay of the excited state (14-17): (i) fluorescence (spontaneous emission), (ii) internal conversion, (radiationless transition between S_1 and S_0), and (iii) intersystem crossing (radiationless transition between S_1 and T_1). Their respective rate constants (s^{-1}) are k_F, k_{IC}, and k_{ISC}. The observed fluorescence lifetime is given by

$$\tau_F = \frac{1}{k_F + k_{IC} + k_{ISC}} \qquad (2)$$

Another important quantity that can be measured is the fluorescence quantum efficiency, Y_F (dimensionless). This is the fraction of molecules that decay by fluorescence from the excited singlet. It can be expressed by

$$Y_F = \frac{k_F}{k_F + k_{IC} + k_{ISC}} \qquad (3)$$

From the observed fluorescence lifetime (s) and the quantum efficiency (dimensionless), the spontaneous radiative lifetime, τ_R, is obtained,

$$\tau_R = \frac{1}{k_F} = \frac{\tau_F}{Y_F} \qquad (4)$$

The radiative lifetime is the lifetime that would be measured if no other processes were involved.

Also of importance is fluorescence quenching. This effect is attributable to many causes, the majority of them being environmental effects. Examples of quenching (14-17)

are: temperature quenching, oxygen quenching, concentration quenching, and impurity quenching. Other environmental effects that are of importance are: solvent effects, heavy atom effects, pH effects, hydrogen bonding effects, and the effects of other solutes. This last effect can be further delineated as the prefilter (inner filter) effect and collisional energy transfer.

In the most analytically useful form, i.e., assuming no prefilter, no postfilter, no self-absorption, monochromatic excitation, the relationship between fluorescence and concentration is

$$I = Y_F I_{EX}(1-e^{-2.303\varepsilon bc}) \qquad (5)$$

where I is the total isotropic fluorescence intensity integrated over all fluorescence wavelengths (relative intensity units), I_{EX} is the intensity of the excitation radiation (relative intensity units), ε is the molar absorptivity coefficient ($L\ mol^{-1}m^{-1}$), b is the sample thickness (m), and c is the concentration ($mol\ L^{-1}$). Other than concentration, there are three major factors that affect the fluorescence intensity: the quantum efficiency, excitation intensity, and absorptivity. If any of these is increased, then the fluorescence increases.

In very dilute solutions, equation (5) reduces to

$$I = 2.303 Y_F I_{EX} \varepsilon bc \qquad (6)$$

Equation (6) indicates that, in dilute solutions, fluorescence

intensity is linear with concentration. At higher concentrations, the fluorescence becomes non-linear, mainly from absorption increasing with concentration. It has been estimated that up to 5% of the exciting radiation can be absorbed by the sample and a linear response obtained (16).

Experimental Approach

To improve the signal-to-noise ratio over that obtained with conventional fluorimetry, a pulsed source-temporal measurement approach was used. The reason for this choice was indicated by previous works reporting the use of temporal measurements to improve analytical determinations (4,18-26), particularly in phosphorimetry.

The pulsed excitation source chosen was a transverse excitation atmospheric (TEA) nitrogen laser. This source has a high peak power and a relatively short duration pulse, as compared to conventional sources. The main drawback of this laser was that the excitation wavelength was fixed at 337 nm, whereas conventional sources, gas filled flashlamps, offered a greater excitation wavelength selection. As a development from the N_2 laser system used, and to be used with the system as an excitation source, an N_2 laser pumped dye laser producing subnanosecond pulses was developed. This dye laser provided a very inexpensive, simple means of obtaining excitation wavelength selection with even shorter pulse durations than that provided by the N_2 laser.

Two separate systems were used for detection and measurement of the temporal fluorescence signals. The first system consisted of a photomultiplier tube (PM) detector and a boxcar signal averager, or sampling oscilloscope, for signal measurement. The second system was a streak camera-SIT vidicon combination. The PM-boxcar system showed greater sensitivity, and hence, lower LOD's (27), but suffered from poor temporal resolution and jitter. The streak camera system offered superb temporal resolution, speed, and ease of use, but suffered from poorer sensitivity and higher cost. The streak camera system was used to observe heavy atom effects on fluorescence lifetimes (4,14-17,28-31) and an attempt was made to demonstrate the utility of the instrument for the time resolution of a mixture of two spectrally overlapping compounds.

Previous workers (32) have demonstrated solvent effects of fluorescence lifetimes, though the analytical use of this type of information is yet to be implimented. Others (18-20, 33-36) have used time resolution as an aid in analysis or to deconvolute two spectrally overlapping compounds.

Fluorescence Temporal Measurements

At the present "state of the art," there are several techniques for the measurement of fluorescence lifetimes. A brief list is presented here, and later in this work. For a more detailed description, refer to Ware (14). The techniques used can be divided into two basic groups, pulsed methods and phase shift methods.

The basis of the pulsed methods is to generate a short, intense, optical excitation pulse and observe the intensity (signal) of the fluorescence decay with time as described in equation (1). The typical excitation source used is a flashlamp giving optical pulses of approximately 1 ns duration (14,16). However, a tailing effect is noted for flashlamps that is not seen for N_2 lasers(37). Recently, mode locked lasers have been used as excitation sources for fluorescence with pulse widths from 1 to 200 picoseconds (38-43).

PM-Boxcar

The most popular, and easiest to use, measurement technique is the sampling oscilloscope used in conjunction with a fast rise time photomultiplier tube as the detector. Suitable PM tubes are commercially available (44-46); however, numerous designs are available to modify less suitable PMs (47-49). Unfortunately, the shorter rise time PM tubes have a lower gain and a significantly increased cost (up to ∿$10,000). Sampling oscilloscopes are available with rise times as short as 25 ps. The use of this combination provides a small portion of the total decay curve with each pulse of the excitation source. To obtain an entire decay curve, the source is pulsed many times. To improve signal-to-noise ratio, many pulses are averaged for each portion of the decay curve. In this averaging mode, the sampling oscilloscope is known by another name, the boxcar signal

averager. Like the sampling oscilloscope, boxcar signal averagers are commercially available.

Transient Digitizer

Also available are transient digitizers, or high speed signal averagers. These operate on the same basic principle as the sampling oscilloscope, except that they sample several different portions of the decay curve per pulse and retain each sampling separately. Hence, an entire decay curve can be approximated with a single excitation pulse, and through averaging, improve the signal-to-noise of the entire decay signal on each pulse. The drawback is that the sampling interval is not as short as that obtained with the sampling oscilloscope, the bandwidth not as high, and the cost is increased considerably.

It should be added that recently a 1 GHz real time oscilloscope has been introduced commercially. Hence, for many fluorescent compounds, an entire decay curve can be obtained real time. The improvement of electronics will continually improve the simplest of temporal measurement techniques and keep it in constant competition with more sophisticated techniques.

Streak Camera

Streak camera techniques are an extension of the transient digitizer methods, except the time resolution is

greatly improved. The principle is relatively simple and very similar to a normal oscilloscope in operation. Under proper timing conditions, the fluorescence is focused on a semitransparent photocathode. Ejected electrons are accelerated and pass between two deflecting electrodes. The relative potential between these electrodes is rapidly swept with time. The electrons ejected at different points in time (corresponding to the decaying fluorescence signal) are deflected further and further. The electrons then strike a phosphor screen and produce a spatially displayed time scan, the fluorescence intensity decay. In most cases, the electrons are amplified just prior to the phosphor screen, increasing the sensitivity of the instrument. A photograph can be taken of this intensity distribution and a densitometer used to obtain lifetimes. In the more sophisticated instruments, a SIT vidicon camera is used and this information passed on to a computer for processing.

The advantages of this technique are that with a single pulse from the excitation source, a lifetime can be approximated, and the time resolution can be as low as 2 ps. The maximum time range is 100 ns, with a temporal resolution of better than 1% of the time range. The disadvantages of this system are lower sensitivity than the sampling oscilloscope - low cost PM method and higher cost. Also, the temporal resolution of a given time range is a difficulty when applying the streak camera to a time resolution separation of a mixture of compounds. Improvements are forthcoming, e.g., a three dimensional temporal scan will be discussed later.

Time-Correlated Single-Photon Counting

Currently, the most popular technique is time-correlated single-photon counting (TCSP) (14,32,33). In this method, fluorescence intensity is reduced to a level such that, at most, only a single photon is detected per pulse. The detection electronics then measure the delay between the excitation pulse and the detected photon corresponding to that pulse. This process is repeated for many excitation pulses, with the number of times that a specific delay is obtained stored in a multichannel analyzer (MCA) preceded by a time-to-amplitude converter (TAC). Each incremental channel of the MCA corresponds to an incremental time delay. After a sufficient number of pulses to insure a good S/N, a histogram showing the number of counts versus delay time is produced. The number of counts in any given time interval is directly proportional to the probability of emission at that time delay. Hence, the histogram corresponds to the fluorescence decay curve.

The important features of this technique are that it is a counting technique, and follows digital statistics, and that it relies on a time difference measurement. This last feature means that this technique depends on the stability and reproducibility of the detection electronics, and not on the analog time response or the ability to reproduce a time-dependent waveform. The temporal resolution of this method depends on the dispersion in the detector and the accuracy

of the deconvolution process, (50,51). Timing uncertainties can be as low as 30 ps (50), and the time range applicable is from 100 ps to 10 μs. One of the problems with this technique is the relatively long data acquisition times; however, improvements are being made. The improvements include higher repetition rate excitation sources, especially mode locked lasers, and better data acquisition systems to operate at the higher repetition rates. Also, this is strictly a lifetime measurement technique; its quantitative and temporal sensitivity is no better than the sampling oscilloscope techniques.

Optical Gating

Optical gating methods, such as the optical Kerr cell, are not widely used for fluorescence lifetime measurements, especially since the methods discussed previously are available. The Kerr cell technique employs a very high power laser to send a pulse through the Kerr cell. The Kerr cell is optically transparent only when the laser pulse is present. Hence, the optical gate can be approximately a picosecond wide, if the proper laser is selected. A portion of the high power laser beam is split off and used to excite the sample in question. The delay between the two pulses is varied by optical delays and the fluorescence decay scanned optically by scanning the optical delay, very much like the electronic scanning of the sampling oscilloscope. The

advantage of this is the time resolution of about 1 ps. The disadvantages are poor S/N, because of amplitude instability of the laser, and a background or scatter also due to the laser, and slow data acquisition due to the low repetition rate of the laser.

Cross-Correlation

An interesting new pulse method has recently been published, implementing a cross-correlation detection system (52,53). The system consists of a mode-locked laser as excitation source and a microwave double-balanced mixer and optical delay as the cross-correlator for a reference laser signal and the fluorescence decay signal. Fluorescence lifetimes as short as 80 ps were measured with ± 10 ps uncertainty. The results obtained, corresponded to those obtained via the sampling oscilloscope techniques.

Phase Shift

Phase shift methods are all based on the relationship that a fluorescent sample excited by a sinusoidally modulated source produce fluorescence signals modulated at the same frequency but with a phase shift relative to the source. This phase shift can be related to the lifetime by

$$\tau_F = \frac{1}{\omega}\tan\theta \qquad (7)$$

for an exponential decay. In equation (7), ω is the

angular modulation frequency ($\omega = 2\pi f$) and θ is the phase shift. The instrumentation needed is some means to modulate the source and a phase sensitive detector.

Light source modulators that have been used are Kerr cells, Pockel cells, ultrasonic modulators, and RF discharges (14). Various phase sensitive detectors have been developed, but generally radio frequency techniques are employed. For example, an instrument has been designed employing a phase-shift null point approach. An optical delay line is used to null the phase while the IF circuitry of an AM radio is used for null point detection (54,55).

Modulation frequencies are limited to approximately 20 MHz, allowing measurement of fluorescence lifetimes from 100 ps to 10 μs. The main disadvantage is that, in the past, only one modulation frequency has been used, corresponding to a single point determination on the fluorescence decay curve. Hence, the reliability is questionable. However, improvements are being made (56,57), such as using more than one modulation frequency for the excitation source.

Power Spectra-CW Laser

A relatively new approach to fluorescence lifetime determinations has been introduced by Ramsey *et al.* (52,58). This approach uses the beat noise of a CW laser as a multifrequency modulated source to obtain the power spectrum of this signal. Hence, it is a frequency determination type of experiment to get temporal information, similar to the

phase shift methods. The disadvantages are low sensitivity, limited lifetime measurement range of from 200 ps to 10 ns, and a large DC background due to the laser, caused by scatter.

CHAPTER II
NOISE POWER SPECTRA OF THE ICP

Introduction

Some of the factors which set limits on precision, accuracy, and limits of detection in chemical analysis are directly relatable to fluctuations recorded in the measurement of the signal. These fluctuations are termed noise (59) and can arise from any point in the total analytical procedure. The fluctuations appear to be random about the mean value of the signal. The smaller the fluctuations (the lower the noise), the higher the reproducibility of the measurement (the better the precision), and the smaller the signal that can be determined (the lower the limit of detection). This also enables a better estimate of the "true" value of the quantity of the analyte corresponding to the measured signal. Hence, determining the noise sources in an analytical procedure, with the hope of minimizing their contribution to the signal is one of the best approaches for improving the analytical procedure (13). In the present work, we are concerned with determining the noise components associated with a popular analytical method, namely the optical system, detection device, and electronic signal processing system of an inductively coupled argon plasma (ICP).

Power Spectrum

To characterize the noise associated with the system chosen, the spectral noise power spectrum (called power spectrum) was determined. The power spectrum indicates the intensity (power) of each frequency component, over a given frequency interval, in the original waveform. It is presented as a noise power per unit bandwidth as a function of frequency ($W\ Hz^{-1}$). It can also be presented as the root-mean-square (RMS) of the noise current per square root bandwidth ($A\ Hz^{-\frac{1}{2}}$), as a function of frequency. Since the noise spectrum displays noise components at their respective frequencies, it can be used in identifying noise sources and to predict their origins. It has been used in the past to find regions of the noise spectrum containing low amplitude noise components into which the information of interest can be transferred, e.g., by modulation (7,60-62), to improve the S/N of the measurement.

Fast Fourier Transform (FFT)

There are both analog and digital methods available for obtaining power spectra. The analog methods used in the past have proved to be tedious and time consuming (6-8), whereas, if a digital computer is available, the digital methods can be implemented rather easily (as attested to in a recent article in a microcomputing journal (63)). There are, also, numerous dedicated instruments available to perform the

computation necessary. These digital computation techniques exploit the Fourier transform properties of the power spectral density function (10). The power spectrum is the Fourier transform of the autocorrelation function, and this was the digital approach used until the advent of the "Fast Fourier Transform" algorithm in 1965 (9). Since that time, the "FFT" has been the method of choice (12) and was the method used here, as implemented by a digital computer.

In using the FFT to determine power spectra, several choices and criteria must be determined. The choices are frequency range to be covered, bandwidth or resolution to be used, and number of data points to be sampled per power spectrum determined. Any two of these parameters specifies the remaining choice. The relation is a simple one

$$\Delta f = f_{MAX} = \frac{(\delta f)(N)}{2} \qquad (8)$$

where Δf is the frequency range, f_{MAX} is the maximum frequency (all measurements always start at 0, or "DC"), δf is the frequency resolution and N the number of data points used.

A criterion that must be met to prevent aliasing is the Nyquist limit. This limit specifies that the sampling rate must be at least twice the rate of the highest frequency of interest. If this criterion is not met, aliasing occurs and information at a higher frequency than the Nyquist limit is "folded over" back onto the power spectrum. In an effort to minimize high frequency information from folding back into a certain frequency range of interest, a low pass electronic

filter is used to attenuate all signals above the highest frequency allowed by the Nyquist limit for a given data sampling. It is also strongly suggested that the sampling rate be chosen such that the highest frequency of interest passed by the filter be near the 3 dB point of the filter, and that both of these be significantly below the Nyquist limit. However, if the sampling frequency is too far below the Nyquist limit then resolution is sacrificed.

At the other end of the frequency spectrum, a high pass filter is suggested to attenuate the very low frequency components. This filter attenuates the signals that appear in the first few resolution elements of the power spectra. The first resolution element, or zeroth harmonic, contains all the power of frequencies from the lowest frequency resolution element to "DC" (10). In some cases, this component could be the dominating feature of the spectrum. If the algorithm used for the FFT requires a scaling procedure, a large DC component could be of extreme importance. The scaling procedure is needed because only a certain number of binary bits are used by the computer in the computation of the FFT, usually one computer word or less. To keep the computer from overflowing its limited word size during the calculation for the FFT, the algorithm constantly checks for overflow errors. If an overflow occurs, usually after an addition or subtraction, the data are scaled by dividing the four (or shifting right twice) and the process during which the overflow occurred, repeated. (It should be noted that

this is only one way to overcome the overflow problem.) In this case, small data values rapidly lose significance. Therefore, it is important to attempt to limit the "DC" (or first resolution element) amplitude by the use of an electronic or digital filter.

It is also possible to do various types of digital processing, or smoothing, either before or after the FFT. Probably, the most important and commonly used digital processing is the selection of a "data window" (10,64-66). In sampling a given waveform, the data are collected for a specified amount of time, giving a representative data set of the waveform. Unmodified, the data were obtained through a rectangular data window. In the FFT, the data window is convoluted with the data, resulting in broadening of the frequency bands and side lobes appearing on either side of a given high intensity frequency component. In an effort to minimize the side lobes, especially where important information is located at a frequency next to a very intense frequency component, the retangular data window is mathematically modified by modifying the data, particularly the data at the beginning and end of the data set. The net effect is to reduce the side lobes relative to the main frequency component. Also, the amplitude of the main frequency component is reduced and the frequency band is broadened, as compared to that obtained with the rectangular data window. (For an excellent discussion of the above, see references (10) and (64,66).)

Noise Components

In previous works (6-8,12,13), the observed noise was broken down into three major groups: (i) white noise, (ii) low frequency (or excess) noise (usually referred to as 1/f noise), and (iii) proportional noise (or whistle noise). White noise is a noise that has a constant amplitude at all frequencies and, as such, forms a baseline for measurements of other noise components above this level. White noise is due to completely random variations in the analytical system. Low frequency noises are noise components that occur at the low frequency end of the power spectrum. In some cases, they follow a 1/f function; hence 1/f-noise has become the more popular terminology. The principal cause for such noise is the slow drift in the instrumental components. This can come about because of temperature changes, changing line voltage, aging of the instrumental components, etc. Proportional noises occur at given frequencies throughout the range of the spectrum. Their cause can be varied, although when noted in flames (12,13), the possible cause was speculated as an "organ pipe" effect; hence the term whistle noise.

Experimental

In Table I, the instrumentation used in this section is given. In Figure (2), a block diagram of the experimental setup is shown. In Appendix A, a flow chart and a description of the FORTRAN program used to manipulate the data is

Table I. Experimental Equipment Used for Noise Power Spectra of ICP.

Item	Model	Source
Computer	PDP 11/34	Digital Equipment Corp. (DEC) Maynard, MA
A/D, D/A	LPS-11	Digital Equipment Corp. Maynard, MA
X-Y plotter, analog	Plotmatic	Bolt, Bernard, and Newman, Inc. Cambridge, MA
Oscilloscope	122 AR	Hewlett-Packard Palo Alto, CA
AC amplifier	103 A	Keithley Instruments, Inc. Cleveland, OH
High voltage power supply	244	Keithley Instruments, Inc. Cleveland, OH
Electrometer	601	Keithley Instruments, Inc. Cleveland, OH
Photomultiplier	R 928	Hamamatsu Corp. Middlesex, NJ
Monochromator	EU-700	Heath-Mc Pherson Benton Harbor, MI
ICP	1500	Plasma-Therm, Inc. Kresson, NJ
Signal generator	180	Wavetek San Diego, CA

Figure 2. Block Diagram of Experimental Setup for ICP Noise Power Spectra

(A) ICP
(B) Monochromator
(C) Capacitor (1 μF, mylar)
(D) PM
(E) High Voltage Power Supply
(F) AC Amplifier
(G) A/D (LPS-11)
(H) D/A (LPS-11)
(I) Minicomputer
(J) Terminal
(K) Analog Plotter
(L) Oscilloscope

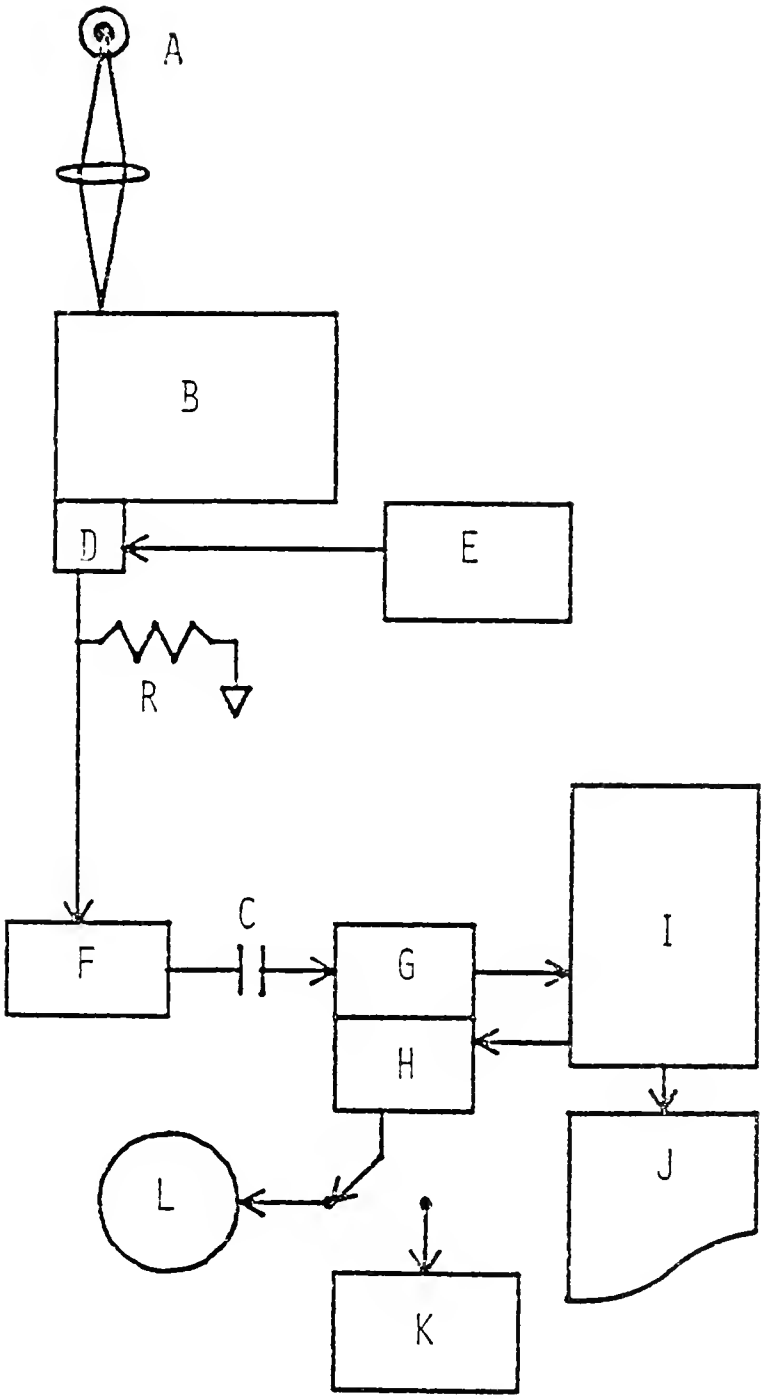
A
B
D
E
R
F
C
G
H
I
J
L
K

given. In Appendix B a flow chart and a description of the fast A/D sampling routine, written specifically for the high frequency range but used for all ranges, is given.

All chemicals used were reagent grade. The chemicals and manufacturers are: zinc metal (Mallinckrodt Chemical Co., St. Louis, MO), barium carbonate (J.T. Baker Chemical Co., Phillipsburg, NJ), lithium nitrate (Fisher Chemical Co., Fairlawn, NJ), and yttrium oxide (American Potash and Chemical Corp., Chicago, IL). Doubly dionized water was obtained from a Barnstead Nanopure water system (Barnstead, Boston, MA).

For each noise power spectrum determined, three different sampling rates were used, 100 Hz, 1 kHz, and 25 kHz. From the Nyquist limit, the frequency ranges covered were, respectively, 50 Hz, 500 Hz, and 12.5 kHz. For each sampling, 2048 data points were collected giving a frequency spectrum of 1024 unique points. Hence, the frequency resolution for the three sampling rates were, respectively, 0.049 Hz, 0.49 Hz, and 12.2 Hz. For the resulting noise power spectra, 100 separate noise spectra were determined and averaged in order to improve the signal-to-noise ratio of the spectra.

The photomultiplier was operated at -1 kV. The Keithley AC amplifier was set to 0.1 Hz for the 3 dB point of the high pass filter in all cases, and the low pass filter was changed as the sampling rate was changed. The roll-off for these filters was -6 dB per octave. The 3 dB point of the

low pass filter was set to 30 Hz for the 100 Hz sampling rate, 300 Hz for the 1 kHz sampling rate, and 10 kHz for the 25 kHz sampling rate. A constant 1000 Ω load resistor was used across the output of the photomultiplier and this voltage signal amplified by the AC amplifier. The output of the amplifier was AC coupled to the DEC LSP-11 A/D converters through a mylar, 1 μF capacitor. This was necessary to reduce the DC offset and drift inherent in the amplifier. The signal gain was adjusted by the gain control on the amplifier in conjunction with changing the input channel of the A/D. The A/D allowed a choice of either ± 1 V full scale input or ± 5 V input, depending on the channel chosen. In all cases, the signal was monitored, prior to sampling, on an oscilloscope to determine which channel to use, such that the great majority of the signal waveform fell within the input voltage limits of the appropriate channel. The channel and gain information was used by the FORTRAN program to scale the data.

The FORTRAN program returned the power spectrum values as RMS current per square root of the frequency bandpass. A calibration curve was obtained using a Wavetek signal generator and the power spectra were found to be linear in amplitude as a function of frequency range and sampling rate to a precision of ± 5 %.

The ICP was operated under normal manufacturer's conditions. A set of parameters was established as a base and various changes were made to note their effect on the noise power spectrum. The base conditions were P = 1.5 kW RF

power, Q = 15 L/min coolant argon gas flow through the torch, N = 1.5 L/min nebulizer flow rate, an observation height (H) of 32 mm above the coil, and 40 ppm Zn sample solution being aspirated (λ = 213.9 nm, slit height (SH) = 1 mm, slit width (SW) = 100 μm). The torch design was similar to that proposed by Genna et al. (67). The DC signal level was measured with a Keithley electrometer. Other values of the P, Q,N parameters were P = 1.0 kW, Q = 20 L/min, and N = 1.0 L/min. Water and 2000 ppm Zn were aspirated also. Another experiment was performed with the same base conditions, but for 100 ppm Ba (λ = 455.4 nm, ion line, SH = 1 mm, SW = 50 μm) and 20 ppm Li (λ = 670.7 nm, SH = 1 mm, SW = 50 μm) aspirated; the corresponding noise power spectra were determined.

A third experiment involved yttrium, 500 ppm, being aspirated (λ = 597.2 nm, SH = 1 mm, SW = 100 μm) and the observation height being varied from 15 mm above the coil to 30 mm, to 45 mm; the noise power spectra were determined at each height.

The torch was changed to the type commercially available and base conditions employed to determine the power spectra from this torch design.

Finally in an attempt to localize the noise sources observed in the power spectra, the nebulizer drain tube was shortened and the base conditions repeated. Also, graphite blocks were placed in the torch cavity such that approximately 50% of the cavity volume was occupied, and the noise power spectra determined using the base conditions.

Results and Discussions

In Table II, the results obtained for the noise power spectra under varying conditions are listed. The table lists white noise amplitude, the frequency and amplitude where the low noise components reach 10% of their peak values (omitting the zeroth harmonic), and any proportional noises, by peak amplitude, frequency, and bandwidth. In Figures 3-12, examples of the noise power spectra obtained are given.

The noise power spectra of only the 500 Hz range is presented in all cases, except where the observation height was varied and yttrium was measured. In that case, the 12.5 kHz range is presented because the low frequency noise appears to extend to significantly higher frequencies at the largest observation height. For all other experimental conditions, the high frequency range offered little information, except to indicate that no other proportional noises existed at higher frequencies. In some cases, the 50 Hz range was not of use because aliasing had occurred resulting in fold over of information from frequencies higher than 50 Hz. This is particularly evident when very strong components are present at higher frequencies.

Figure 13 is an example of the results of this fold over effect. The 50 Hz spectrum of barium corresponds to the 500 Hz spectrum in Figure 10. The broad peak at ∿10 Hz in Figure 13 is due to the peak at ∿210 Hz in Figure 10. Hence, the low frequency information is completely hidden by this high frequency component.

Table II. Noise Components of the ICP With Varying Operating Parameters.

#	Conditions[a]	Frequency Range (Hz)	White Noise Amplitude[b]	Low Frequency Noise 10% Points[c]		Proportional Noise			DC Signal (nA)
				Frequency (Hz)	Amplitude[b,d]	Frequency (Hz)	Amplitude[b,d]	Bandwidth, FWHM(Hz)	
1	IM dark current	50	0.006	0.9	0.05	-	-	-	0.1
2	" (3)	500	0.01	3.4	0.02	-	-	-	0.4
3	H_2O-Base Conditions	50	0.04	1.6	0.3	-	-	-	53
4	" (4)	500	0.1	3.4	0.2	-	-	-	53
5	40 ppm Zn-Base Conditions	50[e]	0.07	19	0.07	-	-	-	135
6	"(5)	500	0.2	22	0.2[f]	210	0.6	10	135
						120	~0.2	-	
7	P=1 kW	50	0.01	11	0.06	-	-	-	19
8	"(6)	500	0.06	20	0.1	-	-	-	19
9	Q=20 l/min	50[e]	0.06	13	0.08	-	-	-	100
10	"(7)	500	0.1	13	0.2	210	0.2	30	100
11	H_2O " Q=20 L/min	50	0.04	0.7	0.1	-	-	-	42
12	"	500	0.09	13	0.1	-	-	-	42
13	2000 ppm Zn[8]	500	2.3	12[g]	2.5	210	24	14	4300
						120	4	-	
14	N=1.0 L/min	50	0.08	8	0.1	-	-	-	230
15	"(9)	500	0.2	11[g]	0.4	195	1.2	10	230

Table II - continued.

16	100 ppm Ba[10] λ=455 nm	500	21	-[b]	-[b]	190	270	11	15000
17	H_2O at λ=455 nm	50	0.62	6	0.04	110	~0.5		
18	"	500	0.03	10	0.07	-	-	-	25
19	20 ppm Li[11] λ=690 nm	500	0.6	68	1.3	240	~0.04	-	25
20	H_2O at λ=690 nm	50	0.03	9	0.07	240	~0.6	-	133
21	"	500	0.02	27	0.1	-	-	-	1.2
22	500 ppm Y, H=45 mm λ=570 nm	500	0.5	-[b]	-[b]	-	-	-	1.2
23	"	12.5 k	0.8	~1 k	1.2	140	-	-	140
24	H_2O-H=45 mm λ=5%	500	0.02	-[b]	-[b]	-	-	-	140
25	"	12.5 k	0.1	-[b]	-[b]	-	-	-	2
26	500 ppm Y, H=30 mm	500	0.1	-		-	-	-	2
27	"	12.5 k	0.5	~1 k	0.6	-	-	-	50
28	H_2O-H=30 mm	500	0.03	-[b]	-[b]	-	-	-	50
29	"	12.5 k	0.1	-[b]	-[b]	-	-	-	4
30	500 ppm Y, H=15 mm	500	0.5	-	-	-	-	-	4
31	"	12.5 k	1.5	-	-	~120 250	-	-	600
						-	-	-	600

Table II - continued.

32	H_2O-H 15 mm	500	0.5	-	-	~120	-	-	460
						~250	-	-	
33	"	12.5 k	1.4	-	-	-	-	-	160
34	40 ppm Zn[12] Commercial torch	500	0.2	-	-	220	1.6	11	150
						120	-	-	
35	H_2O Commercial torch	50[e]	0.01	2	0.04	-	-	-	55
36	"	500	0.1	14	0.1	230	0.1	-	55
37	40 ppm Zn-Short drain	500	0.2	-	-	220	1.5	15	200
						120	-	-	
38	40 ppm Zn-reduced cavity volume	500	0.2	-	-	230	1.5	11	180

(a) Figure number is given in parentheses

(b) All amplitudes are given as $nA/(\text{Bandwidth})^{\frac{1}{2}}$
where for 50 Hz range, bandwidth = 0.049 Hz
for 500 Hz range, bandwidth = 0.49 Hz
for 12.5 k Hz range, bandwidth = 12.2 Hz.

(c) Zeroth harmonic omitted in all data.

(d) The amplitude listed include the white noise amplitude.

(e) Moderate proportional noise at higher frequency which is folded over.

Table II - continued.

(f) Pedestal at 50 Hz used to calculate this value

(e) First harmonic also omitted because zeroth harmonic was extremely large

(b) Indeterminate

Figure 3. Noise Power Spectrum,
PM Dark Current

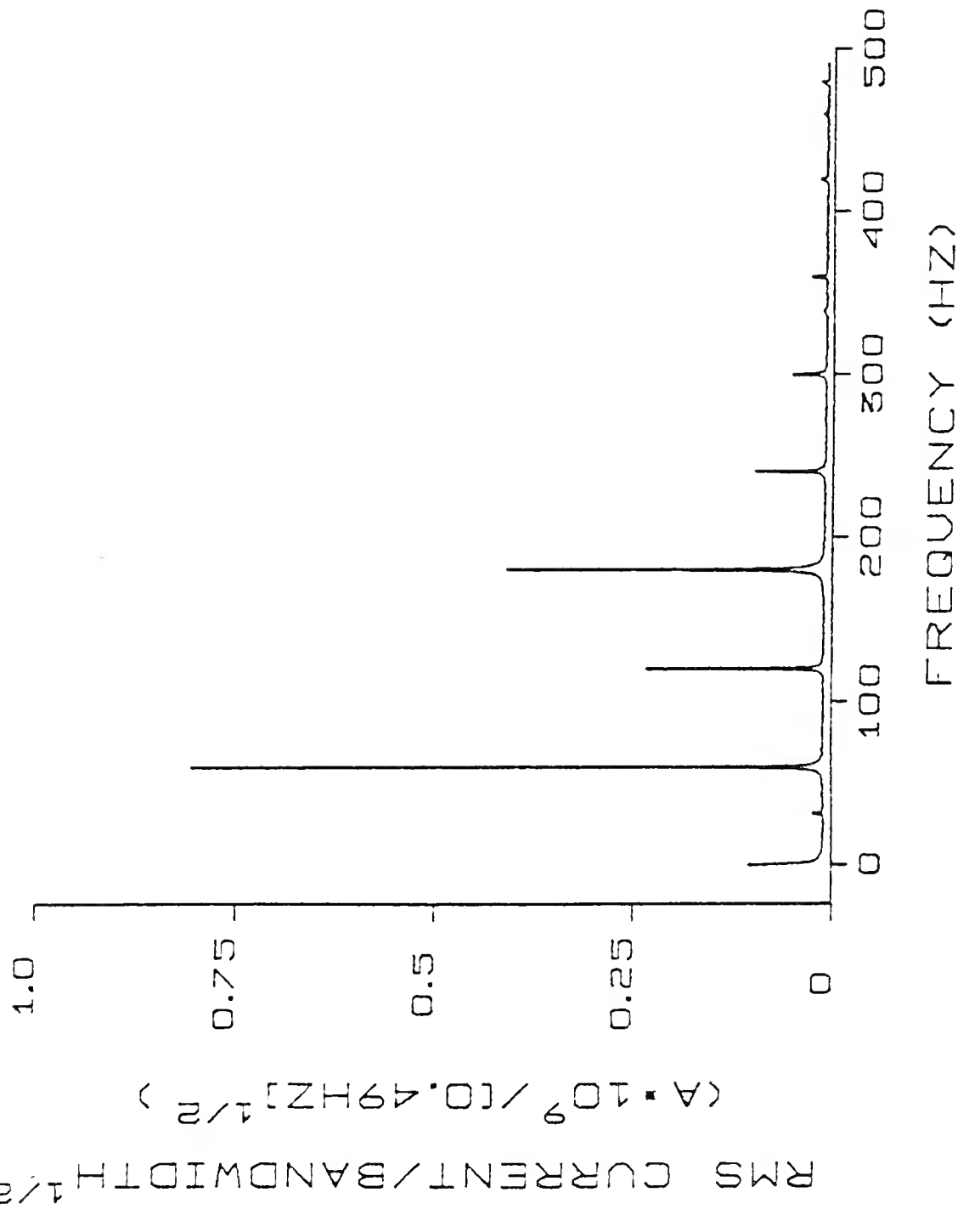
RMS CURRENT/BANDWIDTH$^{1/2}$
(A·10^9/[0.49HZ]$^{1/2}$)
1.0
0.75
0.5
0.25
0
0
100
200
300
400
500
FREQUENCY (HZ)

Figure 4. Noise Power,
Water Background

RF Power (P) = 1.5 kW
Coolant Gas Flow Rate (Q) = 15 L/min
Nebulizer Gas Flow Rate (N) = 1.5 L/min
Observation Height (H) = 32 mm
Slit Width (SW) = 100 μm
λ = 213.8 nm

RMS CURRENT/BANDWIDTH 1/2
(A·10^9/[10.49HZ]^1/2)
2.0
1.5
1.0
0.5
0
0
100
200
300
400
500
FREQUENCY (HZ)

Figure 5. Noise Power Spectrum,
40 ppm Zn

same conditions as
Figure 4
(Base Conditions)

RMS CURRENT/BANDWIDTH 1/2
(A*10^9/[10.49HZ]^1/2)
2.0
1.5
1.0
0.5
0
0
100
200
300
400
500
FREQUENCY (HZ)

Figure 6. Noise Power Spectrum,
P = 1.0 kW

same conditions as Figure 5
except, P = 1.0 kW

RMS CURRENT/BANDWIDTH$^{1/2}$
$(A \cdot 10^9/[10.49HZ]^{1/2})$
1.0
0.75
0.5
0.25
0
0
100
200
300
400
500
FREQUENCY (HZ)

Figure 7. Noise Power Spectrum,
Q = 20 L/min

same conditions as
Figure 5 except,
Q = 20 L/min

RMS CURRENT/BANDWIDTH$^{1/2}$
(A$\cdot 10^9$/[10.49HZ]$^{1/2}$)
1.0
0.75
0.5
0.25
0
0
100
200
300
400
500
FREQUENCY (HZ)

Figure 8. Noise Power Spectrum,
2000 ppm Zn

same conditions as Figure 4

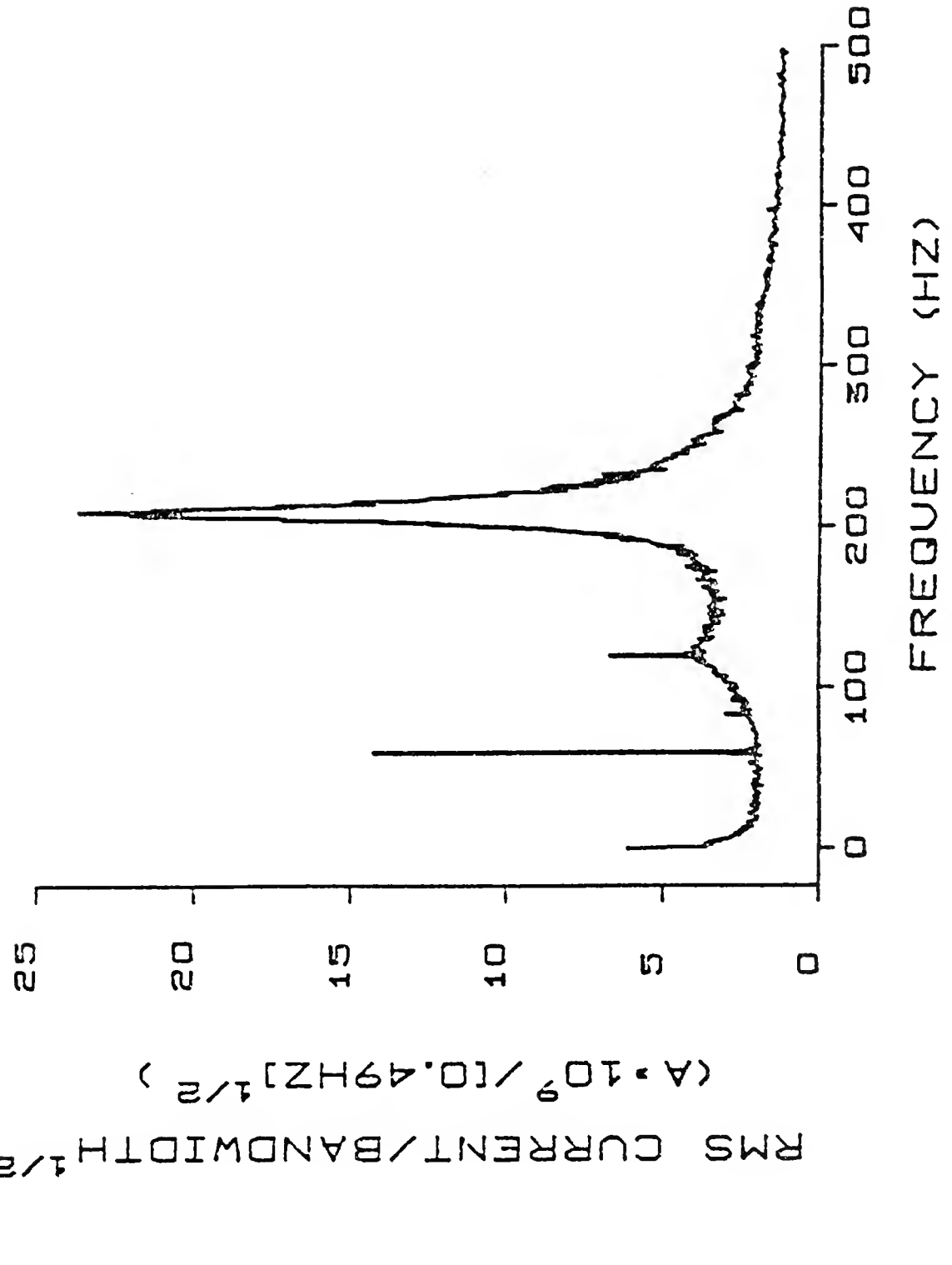
RMS CURRENT/BANDWIDTH$^{1/2}$
(A*10^9/[0.49HZ]$^{1/2}$)
25
20
15
10
5
0
0
100
200
300
400
500
FREQUENCY (HZ)

Figure 9. Noise Power Spectrum,
N = 1.0 L/min

same conditions as
Figure 5 except,
N = 1.0 L/min

RMS CURRENT/BANDWIDTH$^{1/2}$
(A = 10^9/[10.49HZ]$^{1/2}$)
0
1
2
3
4
5
0
100
200
300
400
500
FREQUENCY (HZ)

Figure 10. Noise Power Spectrum,
100 ppm Ba

same conditions as
Figure 4 except,
λ = 455.4 nm,
SW = 50 μm

RMS CURRENT/BANDWIDTH$^{1/2}$
(A * 10^6/[0.49HZ]$^{1/2}$)
0.3
0.2
0.1
0
0
100
200
300
400
500
FREQUENCY (HZ)

Figure 11. Noise Power Spectrum,
20 ppm Li

same conditions as
Figure 4 except,
λ = 670.7 nm,
SW = 50 μm

RMS CURRENT/BANDWIDTH$^{1/2}$
(A*10^9/[10.49HZ]$^{1/2}$)
10
8
6
4
2
0
0
100
200
300
400
500
FREQUENCY (HZ)

Figure 12. Noise Power Spectrum, Commercial Type Torch

same conditions as Figure 5 except different torch design

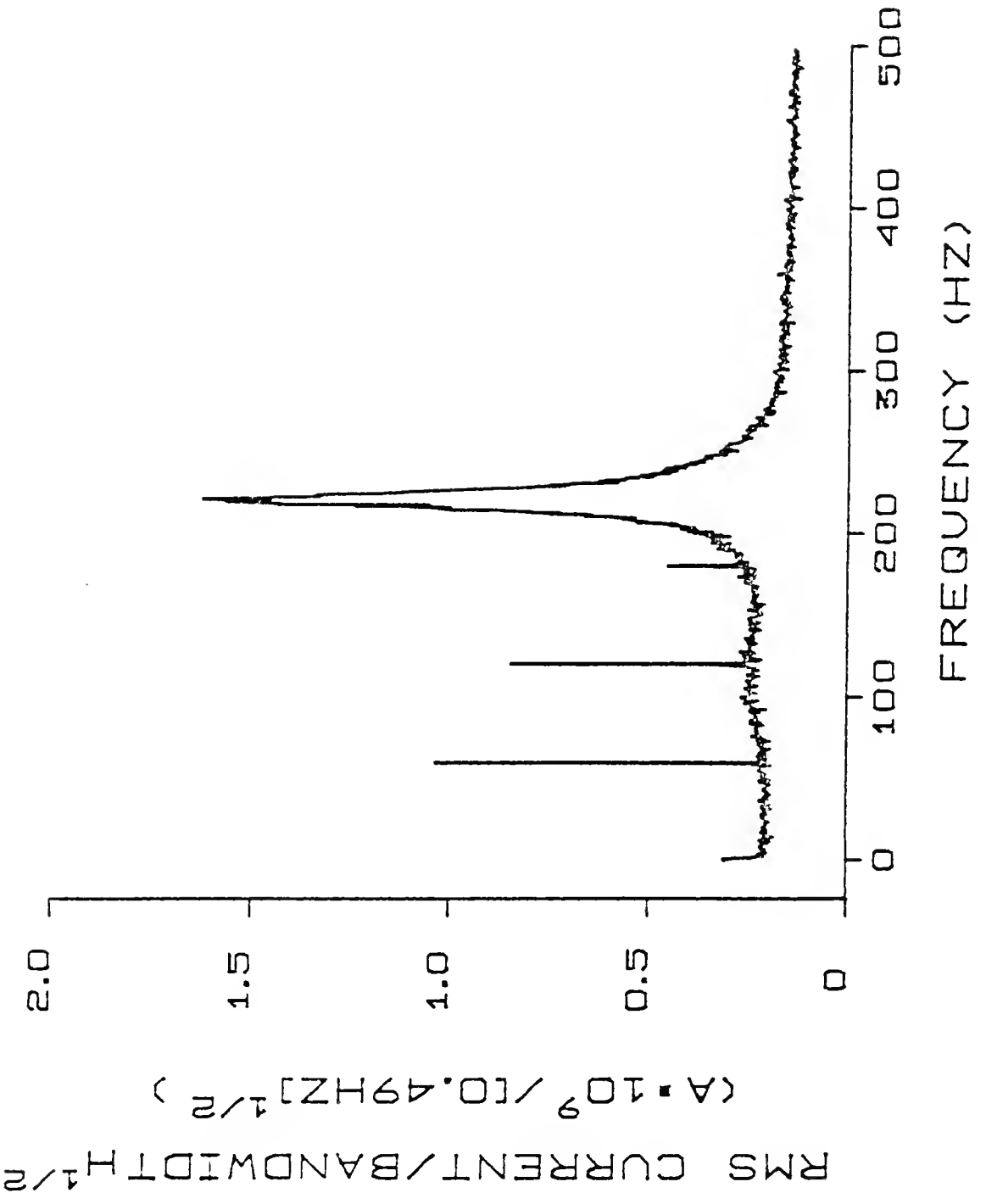
RMS CURRENT/BANDWIDTH$^{1/2}$
$(A \cdot 10^9/10.49HZ]^{1/2}$)
2.0
1.5
1.0
0.5
0
0
100
200
300
400
500
FREQUENCY (HZ)

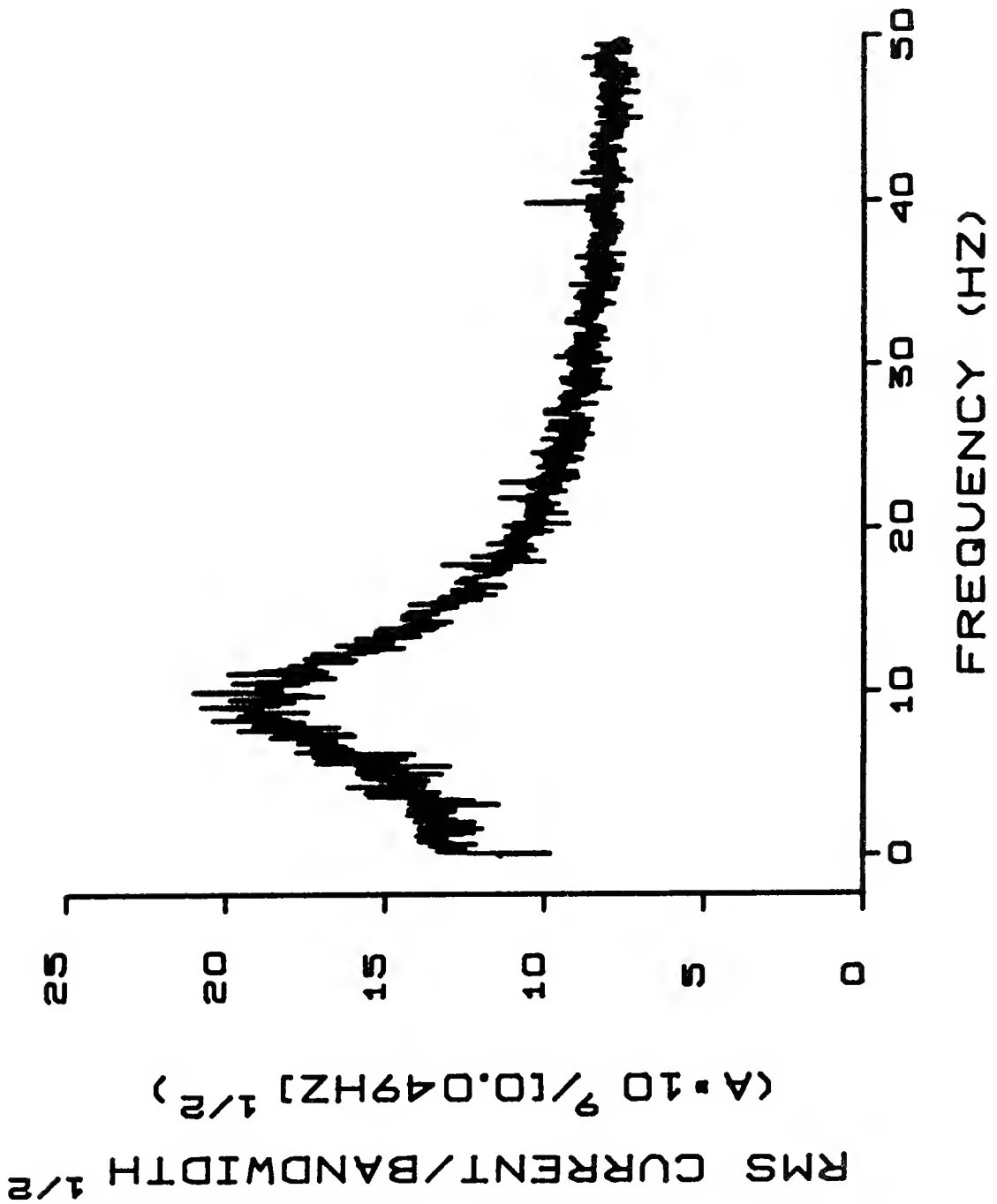
RMS CURRENT/BANDWIDTH 1/2
(A*10 9/[0.049HZ] 1/2)
25
20
15
10
5
0
0
10
20
30
40
50
FREQUENCY (HZ)

The reason for this fold over is that the low pass filter used only attenuated at -6 dB/octave, and for large amplitude signals, this attenuation was not enough. In the 500 Hz range, fold over was probably also occurring, but since there were no proportional noises at higher frequencies, i.e., only white noise, this effect was not observed and not a problem. Whenever information was acquired from the 50 Hz range, the 500 Hz range was checked to determine that there were no large amplitude proportional noises to interfere with this low frequency range.

Spectra

In Figure 3, the noise spectrum of the photomultiplier dark current is shown. This spectrum shows a low frequency component and a contribution from 60 Hz and its harmonics, due to line frequency pickup. It is appropriate to note here that the 60 Hz components were observed in every spectrum and have been recorded previously (13). The change of the relative amplitude of the even and odd harmonics from spectrum to spectrum is also noted. Although the reason for this is unclear, it is believed to be related with the normal operations in the laboratory, i.e., room lights being turned on and off at different times which change the contributions to the different harmonics. However, since these components were constant in frequency, of narrow bandwidth, and determinant, whatever their contribution, they were viewed more

as a frequency calibration than as a hindrance. Also, because of their large intensity, they too were folded over into the 50 Hz spectrum. Again, they were not viewed as entirely detrimental, but as a constant reminder of the aliasing that was occurring.

Another point of interest are the spikes that occur in certain spectra. Even though the spectra presented are the average of 100 separate spectra in each case, miscellaneous spikes, at apparently random frequencies, are observable with good amplitude. The cause of these spikes is not known in all cases; however, in one instance, a major contribution was localized and eliminated as being caused by a poor cable connection from the AC amplifier to the A/D converter. Hieftje and Bystroff (13) also noted spikes in their work which they attributed to sudden aeration of the flame. In Figure 4, a water background of the ICP for the base conditions is given. The only observable noise components, other than white noise, are the low frequency components, which are similar in shape to the dark current components, but they are generally more intense, as is the white noise.

For the base conditions chosen with Zn (Figure 5) as compared to the spectrum obtained with water, white noise increases, the low frequency noise increases and its 10% point (i.e., the frequency at which the low frequency component reached 10% of its maximum amplitude) moves to higher frequency, and, of course, the DC signal increases. Also, a proportional noise is observed at ∿210 Hz, with a less

intense band at ∿120 Hz. Decreasing the RF power decreases the amplitude of the noises as well as the DC signal (Figure 6), as does increasing the coolant gas flow rate (Figure 7), though not as much. Increasing the concentration of the Zn solution being aspirated increased all the noise components as well as considerably increasing the DC signal (Figure 8). Decreasing the nebulizer flow rate also increased the noise and DC amplitudes, though not to the same extent (Figure 9). For barium, at 455.4 nm, the proportional noises, the white noise and the DC signal increased compared to the Zn case while the low frequency noise components became indistinguishable relative to the proportional noise (Figure 10). For lithium, at 670.7 nm, the low frequency noises over the proportional noise components increased and their 10% points occurred at higher frequencies than for the other elements (Figure 11).

Interestingly, very few noise components, other than white noise, were distinguishable with changing observation height at 590.7 nm. However, increasing the observation height, with yttrium being aspirated, extended the low frequency components to a 10% point of approximately 1000 Hz. Decreasing the observation height, with yttrium being aspirated, accentuated the proportional noises.

Changing torches (Figure 12) produced a small shift in the frequency of the proportional noises and greatly increased their amplitude, although the DC signal remained about the same. Changes in drain tube length and cavity volume had little effect on any of the observed noises.

Conclusions

In Table III, the effects of changing the operating parameters of the ICP relative to the base conditions chosen are given. From the change in concentration of the zinc solutions used, it is apparent that the noise components increase in amplitude with increasing DC signal. This is also the case when the RF power was lowered and less DC signal observed. Decreasing the coolant flow rate also increased the signal, and hence, the noise. The same was true for the nebulizer flow rate; decreasing the flow rate increased the signal. This effect can be related to zinc and its residence time in the plasma. Aspirating barium and changing the wavelength to 455.4 nm (near the peak of the argon background of the ICP) seemed to enhance the proportional noises. However, the barium signal was very large. The water background spectrum at this wavelength, compared to that obtained for water at the zinc wavelength, showed a smaller amplitude low frequency component that extended to slightly higher frequencies. This indicates that the low frequency noise was the major component affected by the increase in wavelength. This conclusion was born out when lithium was used and the wavelength changed to 670.7 nm. Here, the major feature is the low frequency noise, even when the water spectrum was determined.

Table III. Summary of the Effects of Changing ICP Operating Parameters Relative to the Base Conditions.

Change mode	Change in DC Signal	Change observed in noise: White Noise Amplitude	Proportional Noise Amplitude	Low Frequency Amplitude	Low Frequency 10% point
Increased analyte cone	+	+	+	+	-
Increased coolant gas flow rate	-	-	-	0	-
Increased wavelength	NA	-	0	0	+
Increased observation height (with Y)	NA	+	-	+	+
Decrease RF power	-	-	-	0	-
Decrease Nebulizer gas flow rate	+	0	+	+	-
Different touch design	0	0	+	-	-

+ = increase

0 = remains approximately the same

- = decrease

NA = not applicable

For yttrium, some interesting effects are noted. The oxide was monitored with the hope of observing changes in the noise power spectrum as the observation height above the coil was changed. The major point noted was, as the height increased, the power in the low frequency components increased. Their 10% point was ∿1000 Hz. The increasing height corresponded to an increase in signal-to-background ratio. When water was aspirated at each height, these low frequency components were not observed. Hence, they were related to the yttrium oxide. This could be an indication of the turbulence in these regions of the torch and the formation of the oxide itself.

When the torch was changed, a slight change in frequency of the proportional noise was noted, but the magnitude of this change was within the variations observed for the torch used in the base conditions. However, the amplitude of the proportional noise was increased substantially which is most likely related to the design change. This "new" torch is the type commercially available; the torch used for the base conditions was of an improved design. The design improvement consisted of constricting the inlet side of the coolant gas tubes giving a greater pressure drop at this point. The results are a more turbulent flow of argon and a reduction in the amount of gas used (67). From the noise power spectra, it appears that the commercial type torch had more noise power in the proportional noises, and the constricted inlet torch had more noise power in the low frequency components.

Thus, the commercial type torch probably has more turbulence at the higher frequencies than does the constricted inlet torch.

An attempt to localize the noise sources by changing the drain tube length and the cavity volume gave no definitive results. The idea of an organ pipe effect (12,13) causing the ∿210 Hz proportional noise indicated a pipe length of approximately 75 cm for a tube open at both ends, and 38 cm for a tube open at one end only, while the torch itself is about 15 cm long. Hence, the attempt at changing the larger volumes associated with the torch.

The large proportional noises shown in the power spectra are readily observable on an oscilloscope. At one point in the trial and error stages of this experiment, a longer torch was tried and a noise component of considerably higher frequency was observed with the oscilloscope. However, that torch was destroyed in one of the many laboratory errors that occur and a replacement was not obtained prior to this writing. It is suggested that the torch design, particularly the length, is responsible for, at least, the frequency of the proportional noises, and contributes greatly to the amplitude of the noise.

The main purpose for these experiments with the ICP was to report noise components at various frequencies in the ICP. In relation to signal-to-noise improvement, the majority of the ICP systems used today are equipped with DC detection electronics employing an integrator or a very low, low pass

filter. Hence, the higher frequency noises will be filtered out. However, at low signal levels, as indicated by the water background spectra, the dominant noise is the low frequency components, the largest of which are passed by the integrator or low pass filter. The extent of their contribution to the "DC" signal measured by the integrator or low pass filter is not clear from the present work and indicates an area of future interest, to characterize the extremely low frequency noises (6,13).

Another region of interest is that of the proportional noise. This "noise" could probably be used as a signal if an appropriate AC amplifier were used. Because of the broadness of the peak, indicating drift or jitter, a lock-in amplifier would not be the system of choice. However, a broad band AC amplifier would certainly be a starting point.

CHAPTER III
FLUORESCENCE TEMPORAL MEASUREMENTS

Introduction

For conventional molecular fluorescence spectrometry, the excitation scatter and luminescence from the blank have been shown to be the major factors controlling the limits of detection. This has also been shown to be the case for laser excited molecular fluorescence (27,68). However, because of their high intensity, an increase in sensitivity (signal/concentration) is often noted with laser excitation. From theoretical calculations (3,69), as well as experimental results, pulsed source excitation with gated detection, using time resolution, could be used to improve S/N in certain instances. Pulsed lasers are very well suited for these measurements because of their high intensities and short pulse widths.

The operating conditions for which the application of time resolution could improve the S/N are important. First, the emission from the analyte and the interfering component, scatter, blank luminescence, etc., should spectrally overlap; otherwise the problem could be spectrally resolved. (This assumes that the interfering component is excited simultaneously with the analyte.) Second, the analyte should have

a significantly longer lifetime than the interfering component, indicating the use of time resolution. If this second point is not true, then the use of time resolution becomes complicated and of little quantitative value. More information is needed about the entire temporal signal and a deconvolution is used to separate the analyte signal from the interfering component. This increase in experimental complexity usually results in a poorer S/N than that obtained with conventional fluorimetry. Other problems result from energy transfer, photodecomposition, etc., and these problems have to be considered on an individual basis to determine if time resolved fluorimetry would offer a more accurate result than conventional fluorimetry.

Time Resolution

The basis of time resolution is shown in Figure 14. The excitation pulse is assumed to be a square pulse, for simplicity. The dashed line is the response of a fluorophor that has a relatively short lifetime. The dotted line represents the response of a fluorophor with a lifetime ten times longer. The remaining dot-dashed line is what would be observed if the two were combined. The principle of time resolution is to allow the short lifetime component to "die out," such that it is contributing very little to the overall signal, and the long lifetime component to dominate. The long lifetime component can then be quantitated with little

Figure 14. Theoretical Approximation of Fluorescence Temporal Response to an Excitation Pulse

(———) Excitation pulse
(- -) Response of component with fast lifetime
(····) Response of component with lifetime ten times longer than fast component
(- · -) Summation of above two components (scaled)

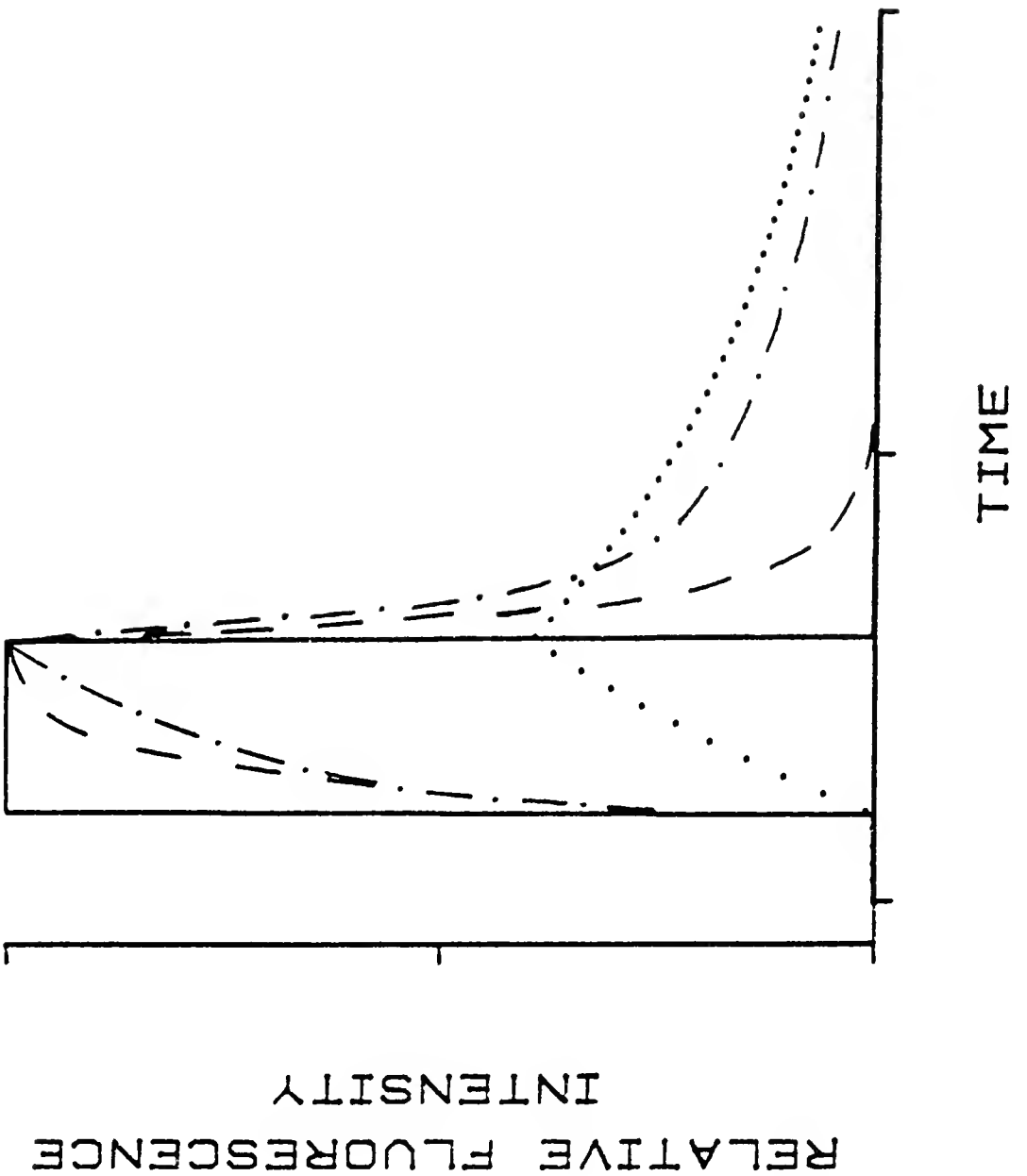
TIME
RELATIVE FLUORESCENCE INTENSITY

interference from the short lifetime component. This has recently been applied analytically to fluorescence (36).

If information is desired about the short lifetime component, more information can be collected from the entire decay of the 2 component mixtures. Once the lifetime of the long lived component is calculated, the intensity (signal) contribution to the overall signal can be estimated and deconvoluted from the total signal, giving the contribution due strictly to the short lifetime component. It is theoretically possible to extend this to more than two contributing species (70-79). However, at the present, the practical limit appears to be the deconvolution of only two spectrally overlapping components (under ideal conditions 3 components could be measured).

If lifetime information is desired, and the relative lifetimes of the two components are significantly different, it is possible to plot the natural logarithm of the signal and obtain a graph that contains two linear regions. The linear region of the graph that has the least negative slope corresponds to the lifetime of the long lived component; the short lived component can then be calculated by deconvolution/subtraction of the long lived component from the total signal as a function of time. An example of this is shown in Figure 15. This is a plot of the natural logarithm of the summation of the two exponential decays shown in Figure 14. The two linear regions are clearly visible. The slope of the lower linear region corresponds to the lifetime of the component

Figure 15. Natural Logarithm of Summation of Two Exponential Decays

(——) Linear plot of the summation of the two responses, shown in Figure 14
(···) Natural logarithm of linear summation

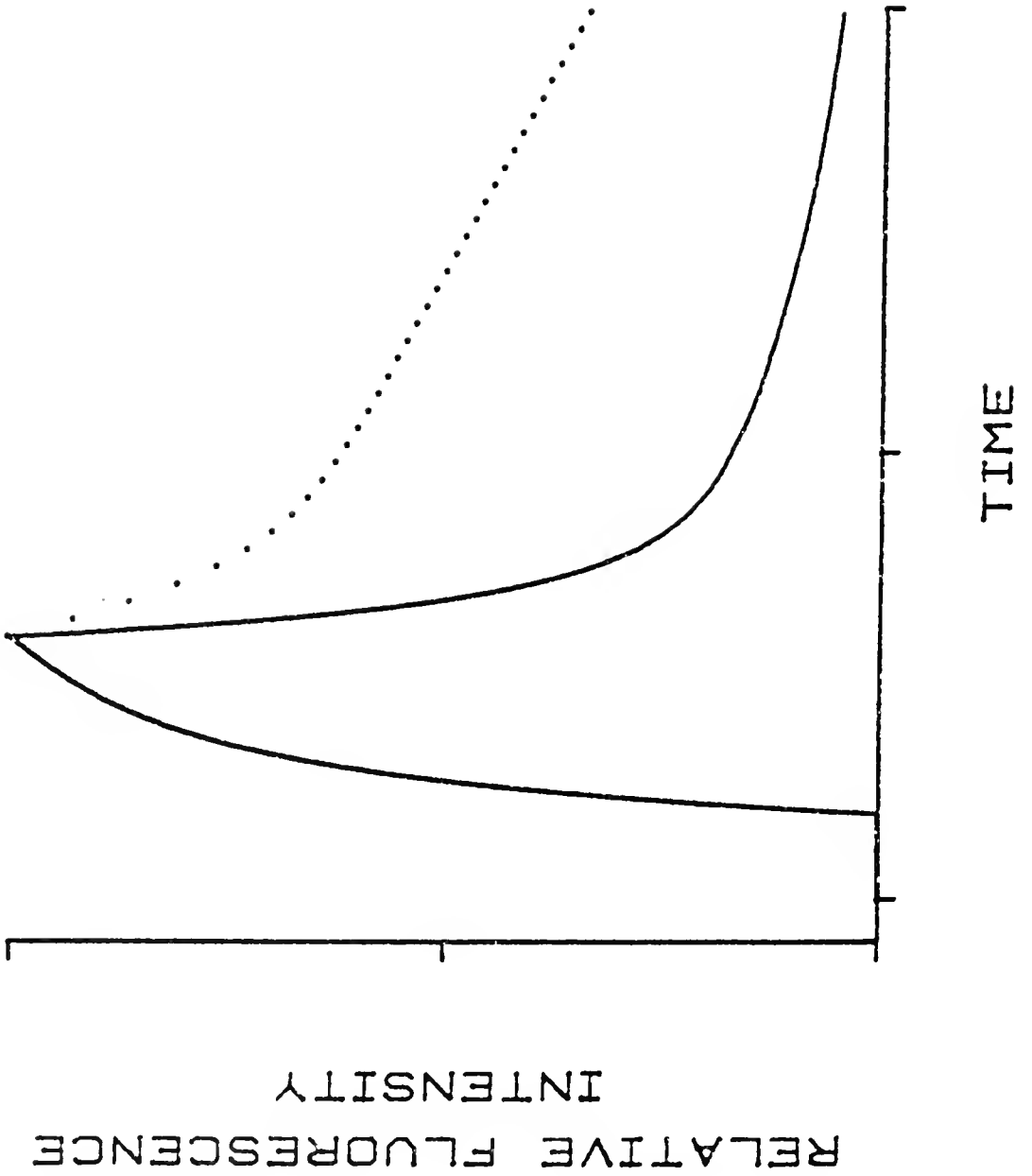
TIME
RELATIVE FLUORESCENCE INTENSITY

with the longer decay time. The upper linear region corresponds to a summation of lifetimes of the two components.

As mentioned previously, there are inherent problems with time resolution. First, the closer the two lifetimes are to each other and/or the greater the signal level of the short lived component compared to the long lived component, the more difficult it is to evaluate the long lifetime component without interference from the shorter lived species. Hence, the information about the short lifetime species is even harder to obtain. Secondly, the further from the laser pulse the decay signal is measured to determine the long lived component, the smaller the signal being measured. Therefore the S/N decreases, even though the relative signal of the long lived component to the short lived component is increasing. Thirdly, what is being observed is fluorescence intensity levels. A large intensity from a short lifetime component makes it extremely difficult to determine a low intensity, long lifetime component. In other words, the relative intensity contributions of the two species can be significantly different only if the relative lifetimes are also significantly different. The reverse case--low intensity, short lifetime component, large intensity, long lived component--is not as susceptible to this problem and time resolution should work better.

An interesting problem that develops from this third point is that, if the quantum efficiency is small for one component and large for the other, then to obtain approximately

equal fluorescence intensities, the concentration of the component with the poorer quantum efficiency must be relatively large. Higher concentrations could lead to quenching and other effects not immediately apparent from the time resolved experiment.

Other problems with time resolution are more subtle, but the experimenter is quickly made aware of some of these. The more important of these subtle problems are generally true of all temporal measurements, especially in the fluorescence decay time range. These are time jitter, drift, pulse to pulse variations, and signal reproducibility. Also, more information is available from the temporal signal than just its application to time resolution. This information is more in the form of a qualitative nature, but with this information it could be possible to improve the quantitative results. Changing the environmental conditions of the sample changes the observed fluorescence lifetime (14-16,32,36,69,80-82). Other effects, such as quenching, photodecomposition, and excited state reactions, could be monitored temporally, providing more information about the sample.

External Heavy Atom

The use of the external heavy atom effect for fluorimetric and phosphorimetric analysis has been demonstrated in the past (4,28-31,83-87). The external heavy atom effect is presumably due to an increase in singlet-triplet

probability from an increase in spin-orbit coupling. The resulting effects reported are, decreased fluorescence intensity, decrease in fluorescence quantum efficiency, decrease in phosphorescence observed lifetime, and an increase in the observed phosphorescence intensity.

The present work shows an attendant decrease in fluorescence lifetimes with increasing concentration of silver nitrate or potassium iodide. The external heavy atom effect on the phosphorescence of two compounds used here has been reported previously (4,31). The external heavy atom effect could be used as a selective means of fluorimetric analysis, as suggested by Zander (28-30). This selectivity could be enhanced with the use of temporal information.

There has been an increase in the interest in the temporal information obtainable via luminescence, as attested to by the reviews by O'Donnell and Solie in 1976 and 1978 (88,89). This interest has grown with the advent of short pulse width lasers and improved detection of events on the same time scale as fluorescence lifetimes or faster. Time resolution as applied to Raman (34,35) or atomic fluorescence (18,19) has been shown to be of considerable use. For phosphorescent species, temporal measurements have been of analytical use for some time (reference 4 and references therein).

With the commercial availability of mode locked lasers and streak cameras, even more interest will be generated in obtaining temporal information (90-92). The analytical use of this information is to be decided in the next decade.

Per Pulse Fluorescence

By being able to determine an entire fluorescence decay on a per pulse basis, as with the use of a streak camera, the temporal information mentioned above is made available rapidly. With greater temporal resolution, pulse to pulse variations are visible and signal reproducability is observable with each pulse. Also, jitter in the time between when the excitation pulse is fired and when the signal is measured can be easily determined, as can the instrumental drift. For most temporal measurement, the only way around such variations is by signal averaging, which tends to blur out the temporal information. If the information is made available on a per shot basis, decisions can be made as to the significance of a particular signal and corrections made to improve the overall signal or averaged signal.

Hence, obtaining the entire fluorescence decay curve per shot of the excitation source, could provide important information about the sample and allow instrumental corrections to give a better measure of the signal.

TEA N_2 Laser

The instrumentation used to obtain the fluorescence temporal information can be quite complex. For the systems used in this work (Figures 16 and 17), the excitation source

Figure 16. Block Diagram of Experimental Setup Using the PM-Boxcar System

(A) Pulse generator
(B) TEA N_2 laser
(C) Sample Cell
(D) PM
(E) Monochromator
(F) High voltage power supply
(G) Boxcar/Sampling oscilloscope
(H) Recorder

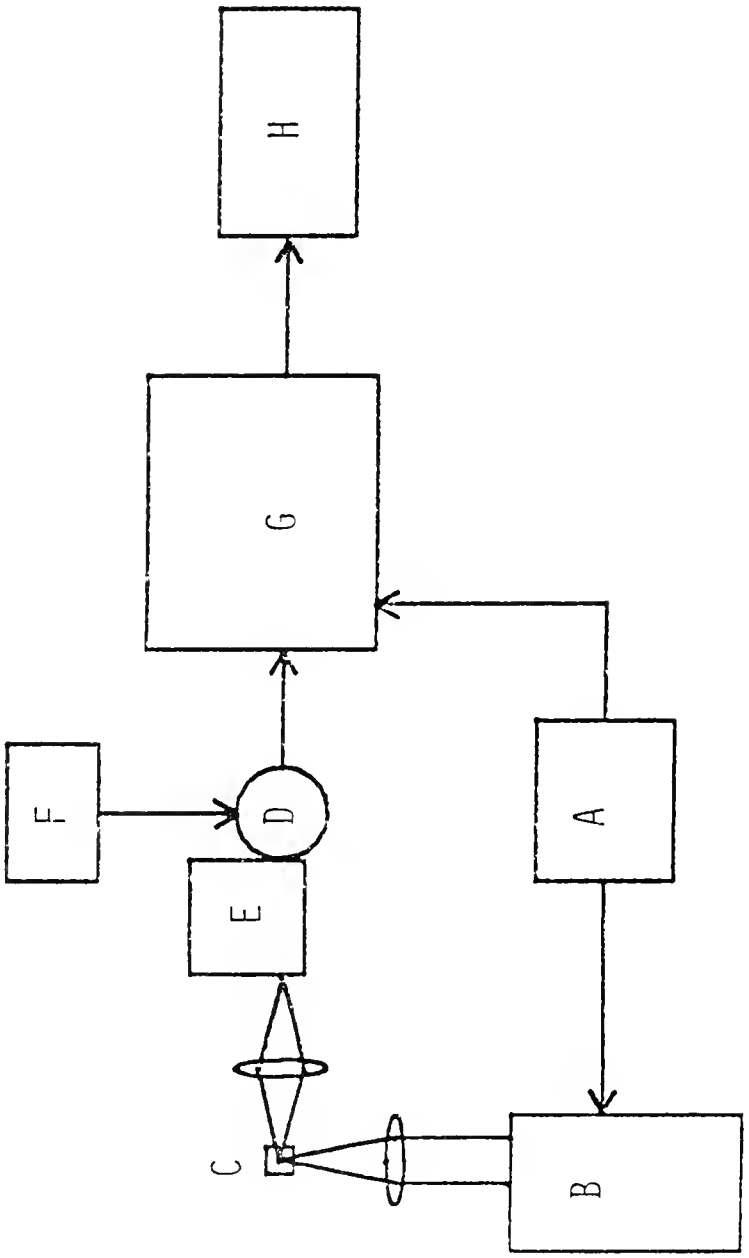
H
G
F
D
A
E
C
B

Figure 17. Block Diagram of Experimental Setup Using the Streak Camera System

(A) Pulse generator
(B) TEA N_2 laser
(C) Sample Cell
(D) Entrance coupling optics
(E) Monochromator
(F) Temporal Disperser (TD)
(G) TD-SIT coupling
(H) SIT-Vidicon
(I) TV controller
(J) Temporal Analyzer (TA)
(K) Monitor, recorder, teletype
(L) Minicomputer
(M) Terminal
(N) Momentary switch

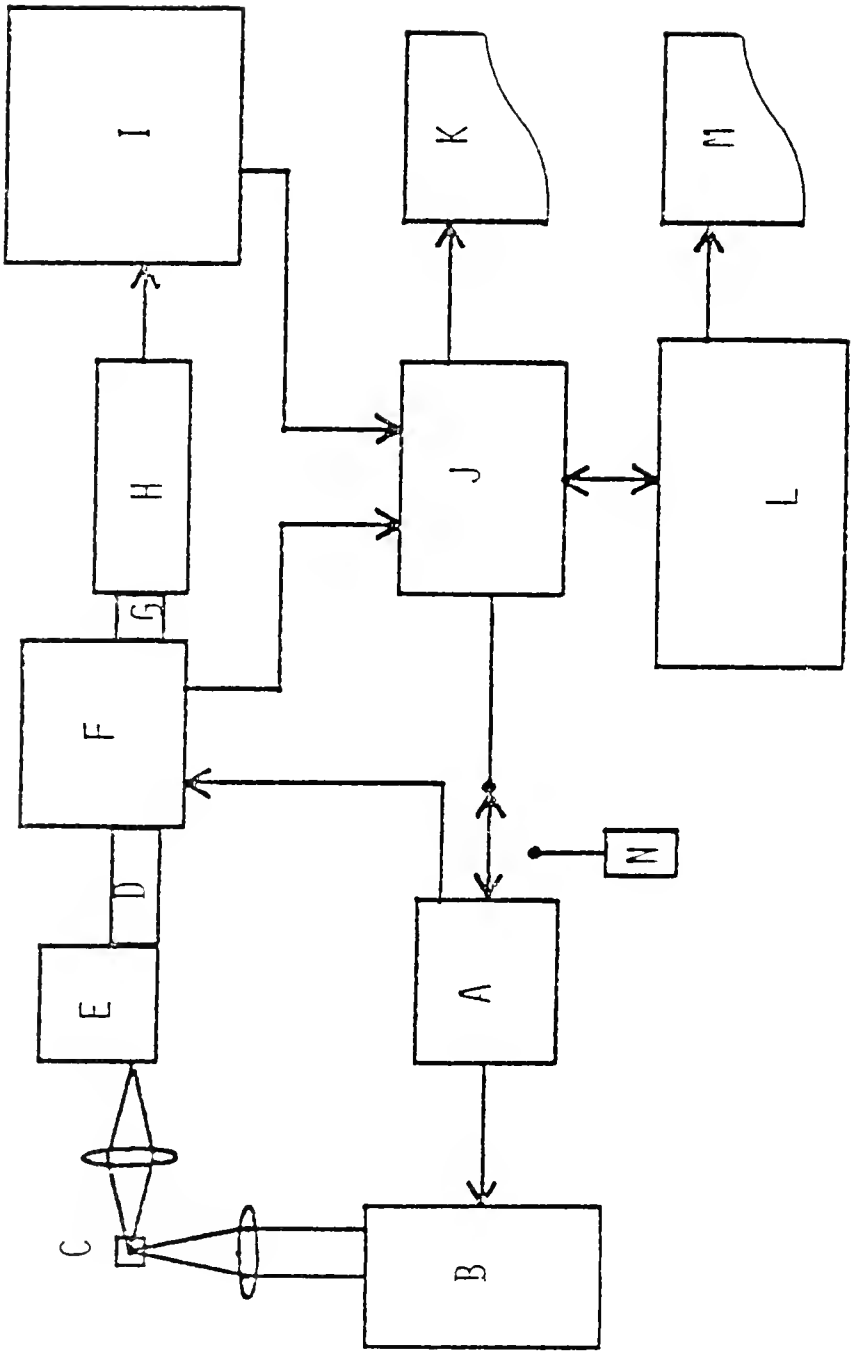
I
K
M
H
J
L
G
F
N
D
E
A
C
B

employed is common to both. This source was a transverse excitation atmospheric (TEA) nitrogen laser. It had a pulse width (measured at full width half maximum, FWHM) of 1.0 ns, a maximum repetition rate of 100 Hz, and an energy per pulse of ∿20 μJ. The TEA N_2 laser is distinctive from the low pressure N_2 laser in that it produces two lines spectrally at 337 nm (93-95). The low pressure N_2 laser produces numerous spectral features (4,95,96). Hence, the TEA N_2 laser is spectrally cleaner offering less problems from scatter due to unwanted spectral features. The TEA N_2 laser also has a shorter pulse width than the low pressure N_2 laser, and it can be made even shorter by using air as the fill gas, instead of nitrogen; however, there is an attendant drop in output power. This means that time resolution can be applied to more systems than if a longer pulse width excitation source was used.

The TEA N_2 laser pulse width is still considerably longer than that produced by mode locked lasers. Also, the excitation wavelength is set at 337 nm. In an effort to reduce the pulse width and increase the variability of excitation wavelength selection, a simple dye laser was constructed which produced pulses as short as 225 ps, FWHM. A more detailed description of this laser will be given in Chapter IV.

The sample cell used was a common fluorescence cuvette, chosen because of the manufacturers claim of being "fluorescence free." In practice, a smaller volume sample cell could

have been used (97). The laser beam was focused into the cell to provide a higher power density and allowing only a small portion of the sample to emit fluorescence. The diameter of the beam entering the sample was approximately 1 mm, giving an illuminated sample volume of about 8 µL. The emission of the sample was focused onto the slit of a monochromator with a simple lens giving a one-to-one image. The maximum slit width was 2 mm, therefore the observed sample volume was about 2 µL. In the optical arrangement used, the slit height of the monochromator was only partially filled with the available sample fluorescence, ≈1 mm. However, in the case of the streak camera, the largest entrance slit to the camera available was 100 µm high and 1 mm wide, so only a small portion of the total fluorescence available was observed. For the PM-sampling oscilloscope/boxcar case, an improvement in the signal level observed could be made if the monochromator slit height and excitation pulse into the sample cell were aligned in parallel.

PM-Boxcar

In Figure 16, the PM-sampling oscilloscope/boxcar system employed is shown. In reality, the majority of the work performed for this section was done using a boxcar signal averager in place of the sampling oscilloscope because it offered a direct method to signal averaging. However, the sampling oscilloscope showed less jitter in the overall

signal measured, for either system, when it was triggered internally (part of the signal used to trigger the sampling head).

The photomultiplier used was wired for fast rise time response (Figure 18). Although other wiring designs are available, as mentioned previously, this design was chosen as a compromise between rise time, versatility, ease of PM replacement, and ease of construction to achieve the desired speeds. It is noted that proper shielding and grounding of the PM was necessary to minimize Radio Frequency Interference (RFI) and ringing of the signal. As such, the PM had a rise time of about 2 ns. Its response to the 1 ns TEA N_2 laser pulse was $\sim$4 ns, FWHM.

The gate widths, or sampling times, used were approximately 350 ps for the sampling oscilloscope and approximately 75 ps for the boxcar. In either case, the system response was limited by the response of the PM. In making the temporal measurements with the boxcar, the laser and the boxcar were both triggered by an external pulse generator. When the sampling oscilloscope was used, and when the signal was large enough, the laser was triggered from the pulse generator and the sampling head was triggered internally. When the signal level was small, the sampling oscilloscope and laser were triggered externally by the pulse generator. In either case, to produce an entire fluorescence decay curve, the sampling gate was internally swept, in time, across the signal. When amplitude measurements were made, the delay

Figure 18. Wiring Diagram of Photomultiplier Dynode Chain

R = 50 kΩ
C = 2 nF

All resistance values are in ohms. All resistors used were carbon film. All capacitance values are in nanofarads. All capacitors are disc ceramic.

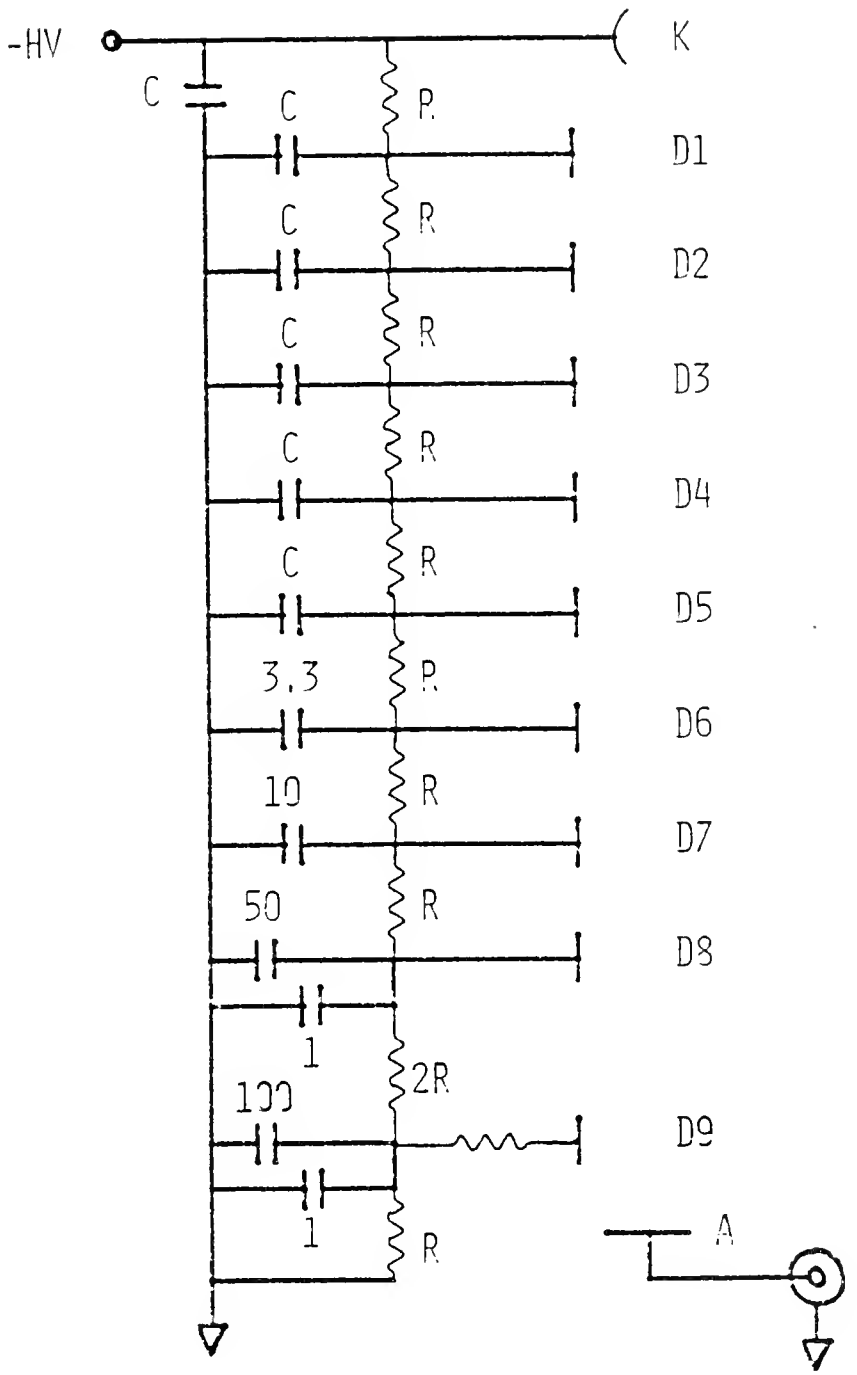
-HV
K
C
C
R
D1
C
R
D2
C
R
D3
C
R
D4
C
R
D5
3.3
R
D6
10
R
D7
50
R
D8
1
100
2R
D9
1
R
A

time from the trigger pulse was fixed. The only variation in the gate position, in that case, was due to jitter or drift.

Streak Camera

In Figure 17, the streak camera system is shown. The temporal disperser (TD) is the actual streak camera and its function is to provide an output exactly described by its name, a spatial dispersion of a temporal event. This output was three dimensional. First, the spatial image of the light passed by the entrance slit is imaged across the output screen in the x direction. This corresponds to the 1 mm slit width. Second, the temporal scan is displayed in the y direction, with the progression of time going from top to bottom of the output screen. Finally, intensity is displayed as the third axis and this corresponds to the fluorescence signal that is being streaked.

To monitor this output from the temporal disperser, a SIT-vidicon camera was used. The vidicon took the three dimensional optical output, converted it to an electronic signal, and passed it to the temporal analyzer (TA), a microcomputer, for processing. The TA was hooked up to a video monitor which provided a real time display of the "streaks" and also a means of outputting the intensity versus time interpretations of this information by the microcomputer. Although the temporal disperser provided three dimensional

output, the temporal analyzer used here only interpreted this information in a limited fashion; the spatial image information was not used. However, the microcomputer added a great deal of versatility to the system. It provided a means of setting up the initial operating parameters of how to handle the information obtained from TD, whether to use a dark current subtraction from the data, how to trigger the system, and how to present the information in the various forms of output (monitor, recorder, teletype, or digitally pass it to another computer).

Computer Link

Finally, in the mode used most frequently for this work, the TA was connected to a minicomputer. This connection was only a one way connection for the transfer of data (with minimal "handshaking" controls) from the TA to the minicomputer. When the system was operated with the minicomputer receiving the data, one streak was performed per data transfer. This allowed the data to be processed by the minicomputer before the next streak occurred. In this way, even more versatility was obtained, and it was possible to make corrections for drift and jitter on a per pulse basis.

Triggering

The triggering of the system was important and varied depending on just how much of the total configuration was

used and what the operating parameters were. Both the N_2 laser and the temporal disperser were triggered by an external pulse generator. After the TD was fired, it, in turn, triggered the temporal analyzer to process the information from the vidicon camera.

The temporal analyzer required about 0.4 s to interpret and display the data on the monitor for a single integration and a persistance of ten (discussed below). If a dark current subtraction was performed, the time required doubled. If the streaks are integrated, the data is acquired at $\sim$0.1 s per shot and the analysis time of 0.4 s, or 0.8 s, is added on. The data transfer through the TA to the minicomputer is done only on a per shot basis and requires the 0.4 s, or 0.8 s, analysis time per shot, depending on whether or not a dark current subtraction is performed before the transfer. With the laser capable of a 100 Hz repetition rate and the temporal disperser capable of following a 1000 Hz repetition rate, it is easy to see that the temporal analyzer is the rate determining step in the total data acquisition process.

When the pulse generator is triggered internally, the laser and temporal disperser can produce information at a rate up to 100 Hz. However, the TA can not handle such a large throughput. (It should be noted that the vidicon camera provides one complete frame every 17 ms, so it could not follow this rate either. But up to a repetition rate of 60 Hz, the monitor displays the streaks as the vidicon collects the information. Hence, the time consuming process

is the interpretation of the temporal information by the microcomputer.) This is the reason for driving the pulse generator externally.

With the pulse generator triggered externally, it is possible to "single shot" the system using a momentary switch or to have the TA trigger the pulse generator after each data analysis. The last technique is the most efficient in terms of analysis time. It also keeps photodecomposition to a minimum and reduces the aging of the laser. For most of the work presented here, this is the triggering technique used. During the initial setup, the system was free run (pulse generator on internal) or "single shot."

Another modification is to have the laser free running and "single shot" the temporal disperser or have the TA gate the temporal disperser such that it only obtains a streak after the microcomputer was ready. Problems here include an increase in the possible photodecomposition per analysis, triggering of the data acquisition is not optimized, and an overlap of streaks, before analysis, if the triggering rate of the laser is too high.

Computer Routines

For the analysis of lifetimes and pulse widths of lasers, averaging was important to improve the S/N, hence the mode of data transfer to the minicomputer was used. Several types of data processing routines were tried to overcome the

problems of jitter and drift. The two that were the most useful were a "step seek" routine and a "peek seek" routine. The step seek routine was used mainly for the fluorescence temporal measurements. With the pulse width of the excitation source being 1 ns, or less, the rise time of the pulse was considerably faster. In most cases, the growth of the fluorescence signal was faster than the signal decay, because of the excitation pulse. Hence, the fluorescence signal had a relatively sharp leading edge. The step routine seeks out this leading edge as it crosses a specified threshold value, and adjusts each data set such that they are all added together from this point.

The peak routine was used mainly for the pulse width measurements of the lasers tested, in conjunction with a single shot measurement. This routine scanned the data sets for their maximum values and added each data set together such that the points in time where maxima occurred overlapped.

SIT Camera

With the use of the vidicon camera, one has to be careful to work with certain inherent characteristics (98-101). For the work reported here, the most important characteristic to be aware of is the persistence of the camera itself. It has been found that for the best S/N, several frames of video signal should be summed together after a streak to deplete completely the charges on the silicon target (102). As far

as the signal gain is concerned, the temporal disperser is the limiting element, not the vidicon. The reason for this is intuitively simple: if the light intensity is too low for the temporal disperser to produce an output signal at its phosphor screen, then the vidicon will not produce a signal either.

With the temporal disperser used in this work, two plug-in electronic modules are available, which determine the streaking speeds. Four ranges are available on each plug-in, 1,2,5, and 10 ns full scale for the high speed plug-in, and 10,12,50, and 100 ns full scale for the slow plug-in. The temporal resolution is stated as better than 1% for each range on each plug-in. For the work presented here, only the slow speed plug-in was used because of the pulse width of the excitation source.

An added feature only on the slow plug-in, is the "finder mode." This expands the streak range, non-linearly, and is useful in finding the temporal signal and adjusting delays such that the streak, in the normal operating mode, will appear on scale. In the finder mode, the temporal signal can be adjusted so that it occurs totally at the top or bottom of the streak, the TD being triggered after or before the temporal signal, respectively. Hence, the signal is shoved together giving little temporal information but a larger signal level than that obtained if a normal streak was made. For quantitative information, this mode of operation should give lower limits of detection.

Experimental

In Table IV, the instrumentation used in this section is listed. In Figures 16 and 17, the block diagrams of the experimental setups are shown. Appendix C gives the flow chart and description of the FORTRAN program used to manipulate the data transferred from the TA. Appendix D gives the flow chart of the assembly language program supplied with the streak camera system, the modifications made to get the program to work, and a description of the handshaking that was used for the two computers to communicate.

All chemicals used, listed below, were reagent grade and were used without further purification:
perylene, rubrene, pyrene, fluorene (Chem Service, West Chester, PA); anthracene (Matheson, Coleman, and Bell, Norwood, OH); phenanthrene, 7,8-benzoflavone (Eastman Kodak Co., Rochester; 1,2,5,6-dibenzanthracene, riboflavin (Nutritional Biochemical Corp., Cleveland, OH); cephradine (Squibb and Sons, Princeton, NJ); primaquine phosphate (Sigma Chemical Co., St. Louis, MO); quinine HCl (Aldrich Chemical Co., Inc., Milwaukee, WI); quinine sulfate, Standard Reference Material (National Bureau of Standards, Washington, D.C.); silver nitrate, potassium iodide, n-heptane, hexane (Mallinckrodt Chemical Co., St. Louis, MO). Doubly deionized water was obtained from a Barnstead Nanopure water system (Barnstead, Boston, MA).

Table IV. Experimental Equipment Used for Temporal Measurements.

Item	Model	Source
TEA N_2 laser	SP1/2	Garching Instruments - available through Interactive Radiation, Inc. Northvale, NJ
Monochromator	H-10-V	ISA Metuchen, NJ
Photomultiplier	R 777	Hamamatsu Corp. Middlesex, NJ
Temporal dispenser	C 979	Hamamatsu Corp. Middlesex, NJ
Slow plug-in	M 1284	Hamamatsu Corp. Middlesex, NJ
Vidicon camera and controller	C-1000-12G	Hamamatsu Corp. Middlesex, NJ
Temporal analyzer	145	Hamamatsu Corp. Middlesex, NJ
Pulse generator	111	Tektronix, Inc. Beaverton, OR
Oscilloscope	545A	Tektronix, Inc. Beaverton, OR
Sampling head	151	Tektronix, Inc. Beaverton, OR
Boxcar signal averager	162/163/ Tektronix S2 head	EG & G, Princeton Applied Research Princeton, NJ
Minicomputer	PDP 11/39	Digital Equipment Corp. Maynard, MA
D/A	LPS-11	Digital Equipment Corp. Maynard, MA
Stripchart recorder	SRG	Sargent-Welch Skokie, IL
X-Y plotter	Plotmatic	Bolt, Bernard & Newman, Inc. Cambridge, MA

Table IV - continued

High voltage power supply	244	Keithley Instruments, Inc. Cleveland, OH

Using the laboratory wired photomultiplier tube base (Figure 18), the temporal response of several PM tubes, to the N_2 laser pulse, was obtained. The PM tubes used were two 1P28s (RCA, Lancaster, PA); EMI 9781B (EMI, Plainview, NY); R777, R212UH, and three R928s (Hamamatsu Corp., Middlesex, NJ). Also tested was a specially wired 1P28 obtained from Dr. Fred Lytle (Purdue University, West Lafayette, IN). The output signal, in each case, was fed into the boxcar signal averager to obtain the temporal scan. Results were compared with that obtained from an ITT biplanar vacuum photodiode (ITT, Fort Wayne, IN), rise time $\leq$ 500 ps. All detectors were operated at -1000 V.

For the solutions used, no degassing was performed prior to analysis. The N_2 laser was triggered at 100 Hz when the PM-boxcar system was used. When the streak camera system was used, 100 laser shots were averaged to obtain the temporal information at a rate of $\sim$1 Hz.

Results and Discussion

PM-Boxcar

For the laboratory constructed photomultiplier tube base, all PMs tested gave about the same temporal response to the N_2 laser, a function of the base. However, the signal gain varied significantly. The two 1P28s gave the largest and the smallest signal responses, the difference being approximately a factor of four. Dr. Lytle's PM gave the

fastest temporal response, but the signal gain was lower than that obtained with the worst 1P28 tested by a factor of 2 to 3. This is probably because the optical coupling used was not the same as that for the laboratory constructed base. The base design of Dr. Lytle's PM made housing the tube and coupling it to existing equipment difficult. It was even more difficult to replace the PM itself. This action became necessary when the original PM was found to be arcing out, which destroyed the sampling head. Hence, for these reasons, the laboratory constructed base was used for all further work, incorporating the R777 photomultiplier tube. The signal gain of the R777 used was down a factor of two from the best 1P28, but the R777 has an extended spectral response.

The temporal information that was obtained with the PM-boxcar combination suffered from several problems. Most important was the response of the PM itself. With a response to the N_2 laser of $\sim$4 ns, any signal faster than about 5 ns would be difficult to distinguish from the PM response and a deconvolution would be necessary. With large signals, it is also possible to saturate the PM (103,104), even though the average current is below that specified for the tube and the tube is specially wired for pulse work. Here, saturation is the space charge limitations of the last few dynodes of the PM. Essentially, trying to get more current out of the tube than is possible. Saturation causes a signal that is non-linear with the light flux to be measured. Also, the

temporal information is distorted or lost. In Figure 19, an example of PM saturation with anthracene is given. Temporal scans at several wavelengths were made to ensure that the observed effect was not excitation saturation of the compound, i.e., "equalization" of the populations of the energy levels involved in the excitation process.

Other problems inherent with the boxcar system for the shortest time range (0-100 ns) were, ± 2 ns accuracy in the delay range setting, ± 3 ns linearity of the delay range, jitter of the overall system of 0.5 ns, and an overscan of approximately 7 ns, when used in the scanning mode (105). Therefore, when used for time resolution, where a minimum of two measurements are needed for each sample, the error in the temporal measurement could be as large as ± 7 ns. This is about the maximum error expected if a signal is scanned. Hence, caution should be used in interpreting the temporal information obtained with the boxcar. Experimentally, in our studies, the PM response was the limiting temporal resolution element.

In Table V, the fluorescence lifetimes obtained with the PM-boxcar system are listed. For all values reported, the lifetimes were measured approximately 10 ns after the time corresponding to the peak intensity. This was to insure that the excitation pulse was not substantially contributing to the lifetime measurement, i.e., it had essentially died out. The values obtained are in reasonable

Figure 19. Photomultiplier Saturation with Anthracene Fluorescence at Various Wavelength

(A) λ = 505 nm
(B) λ = 476 nm
(C) λ = 445 nm
(D) λ = 420 nm

Signals obtained with PM-boxcar System
60 ns full scale

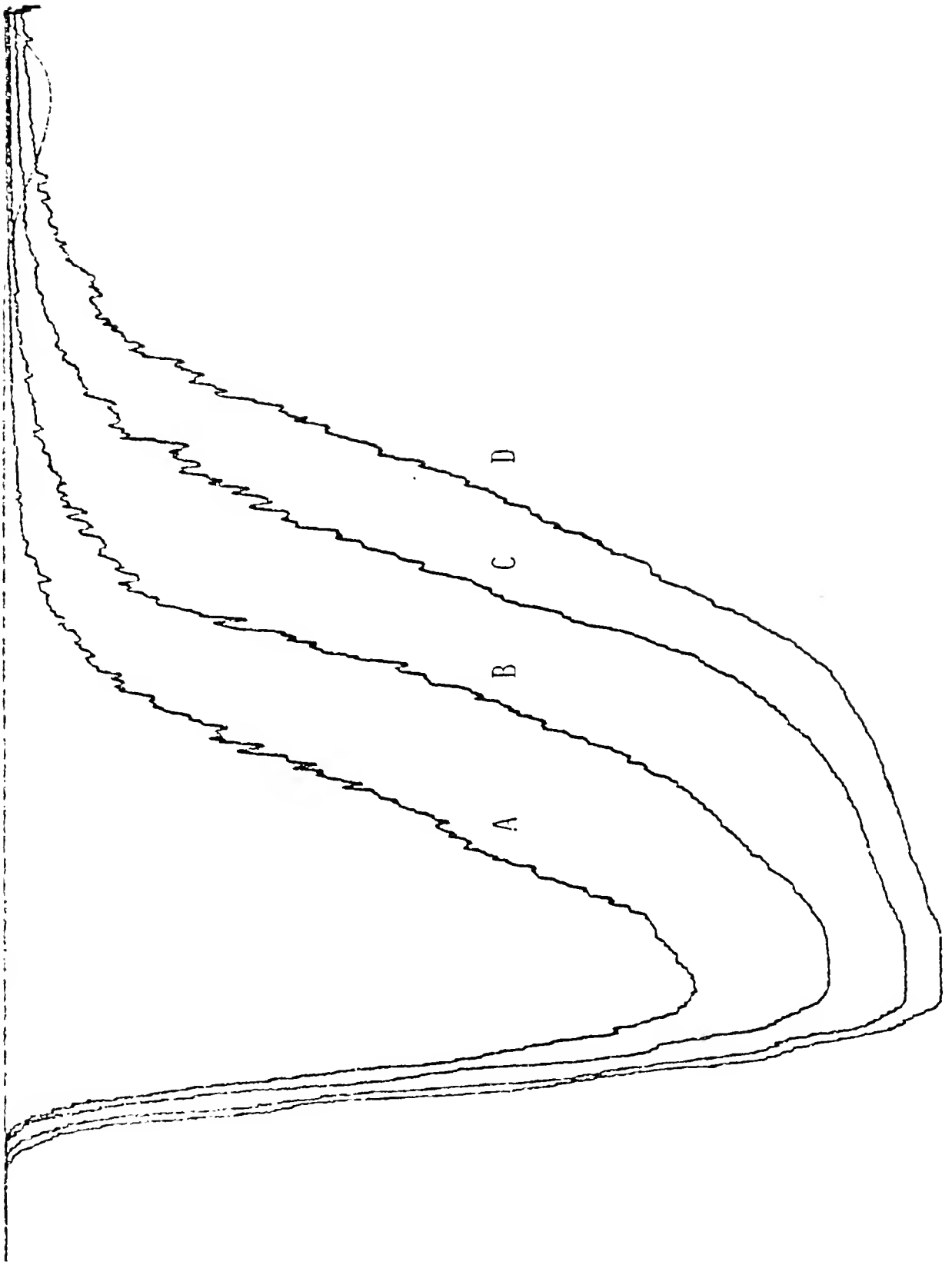
A
B
C
D

Table V. Fluorescence Lifetimes Measured with the PM-Boxcar System.

Compound (solvent)	τ(ns) This work[a]	Literature values[b]
phenanthrene (n-heptane)	6	71[d] (107)
pyrene (n-heptane)	11	400[d,e] (107)
rubrene (n-heptane)	12	16 (16)
anthracene (n-heptane)	4	4.9 (106) 5.75 (16)
quinine HCl (1 N H_2SO_4)	22	19.2 (106)[c] 15.2 (16)[c]

(a) Values reported are to ±7 ns.

(b) References are those given in List of References.

(c) quinine sulfate.

(d) These values were obtained under very different conditions than that used for this work.

(d) Also see Table VI.

agreement with those reported previously, taking into consideration the possible error limits of the measurement system.

For the temporal analysis of fluorescence decays on the 1 to 10 ns scale, the PM-boxcar system used here is not well suited. It is, however, suited for the range from 10 ns to 200 ns. Above this time range, the scanning times required would be inordinately long to achieve the desired S/N, because of the 75 ps gate width. For example, the maximum scan rate for the 200 ns range at a repetition rate of 100 Hz with the minimum signal averaging is ∿1 min. To improve the S/N a factor of 10 would require ∿100 min to cover this same range at 100 Hz repetition rate. For single point measurements, the system is quite excellent with jitter on the order of 0.5 ns and drift about 0.2 ns/min.

Streak Camera

In Table VI, lifetimes measured using the streak camera system are given. Table VII gives the lifetimes measured with external heavy atoms present. The results were obtained to a greater precision (± 0.1 ns) than with the PM-boxcar system, because the drift was less and the jitter was partially compensated for in the data collection system. A least squares program was run on the natural logarithm of intensity versus time data to obtain the lifetimes (the negative inverse of the slope of the least squares line). In

Table VI. Fluorescence Lifetimes Measured with the Streak Camera System.

Compound	τ(ns) this work[a]	literature[b]
quinine sulfate (SRM), 1 N H_2SO_4	19.5	19.2 (106)
quinine HCl, 10% ETOH/H_2O	20.0	
quinine sulfate, ETOH	18.7	
riboflavin, 10% ETOH/H_2O	4.4	4.2 (16)
perylene, ETOH	5.7	6.4 (106)
perylene, n-heptane	4.3	
pyrene, hexane	11.1	
1,2,5,6-dibenzanthracene, ETOH	13.0	
1,2,5,6-dibenzanthracene, n-heptane	8.5	
fluorene, hexane	3.8	
anthracene, n-heptane	3.8	4.9 (106)
anthracene, hexane	3.0	
anthracene, 55% ETOH/H_2O	4.7	
rubrene, n-heptane, λ=556	11.2	16 (16)
rubrene, n-heptane, λ=415	2.9	
cephradine, 50% ETOH/H_2O	1.4	
primaquine, 10% ETOH/H_2O	1.3	
7,8-benzoflavone, 10% ETOH/H_2O	2.1	

(a) Values reported are to ±0.1 ns.

(b) References are those given in List of References.

Table VII. External Heavy Atom Effect on Fluorescence Lifetimes.

	Fluorescence Lifetimes (ns)		
Concentration (M)	Riboflavin (11.2 ppm, λ=530 nm, 10% ETOH/H_2O)	Quinine HCl (18.5 ppm, λ=445 nm, 10% ETOH/H_2O)	7-8-Benzoflavone (15 ppm, λ=439 nm, 10% ETOH/H_2O)
$AgNo_3$			
10^{-4}	4.7	18.8	2.0
10^{-3}	4.9	19.4	2.0
10^{-2}	4.4	19.7	1.9
10^{-1}	3.0[a]	8.0	1.5
KI			
10^{-4}	4.6	19.5	2.1
10^{-3}	4.7	13.7	1.9
10^{-2}	3.4	4.0	1.6
10^{-1}	1.8[a]	1.0	0.9
no heavy atom	4.4	20.0	2.1

(a) 5×10^{-2} M heavy atom perturber.

Table VII - extended.

Anthracene (20.5 ppm, λ=420 nm, 55% ETOH/H_2O)
4.5
4.6
3.9
2.6[a]
4.6
4.8
4.0
2.5[a]
4.7

Figure 20, an example of the fluorescence decay of quinine sulfate in 1 N H_2SO_4 is given. The natural logarithm of this data (dotted line) is also presented.

Fluorescence Lifetimes

The lifetimes found here are in good agreement with those reported previously (16,106,107); each lifetime was processed in a little over 1 min. Hence, this is an excellent system for the determination of fluorescence lifetimes with two exceptions. The major problem is that the excitation wavelength is set at 337 nm. Therefore, a large number of compounds can not be excited. Also, the pulse width of the laser is the limiting temporal element, without resulting to deconvolution. This limits the measurable fluorescence lifetimes to approximately 1 ns or greater. These limitations are directly related to the TEA N_2 laser used. By the use of an excitation source with a shorter pulse width and variable wavelength, especially in the UV, shorter fluorescence lifetimes and the lifetimes of more compounds could be measured. A solution to this problem would be a mode locked, cavity dumped, synchronously pumped dye laser with a frequency doubled output. Presently, this type of excitation system produces pulses of relatively low power and is quite expensive; even more than the streak camera.

The approach taken here to overcome the limitations of the N_2 laser was to develop an inexpensive dye laser system

Figure 20. Quinine Sulfate Fluorescence Temporal Response to TEA N_2 Laser and Natural Logarithm of Decay

(——) Linear fluorescence signal
(···) Natural logarithm of fluorescence decay

Obtained with Streak Camera System

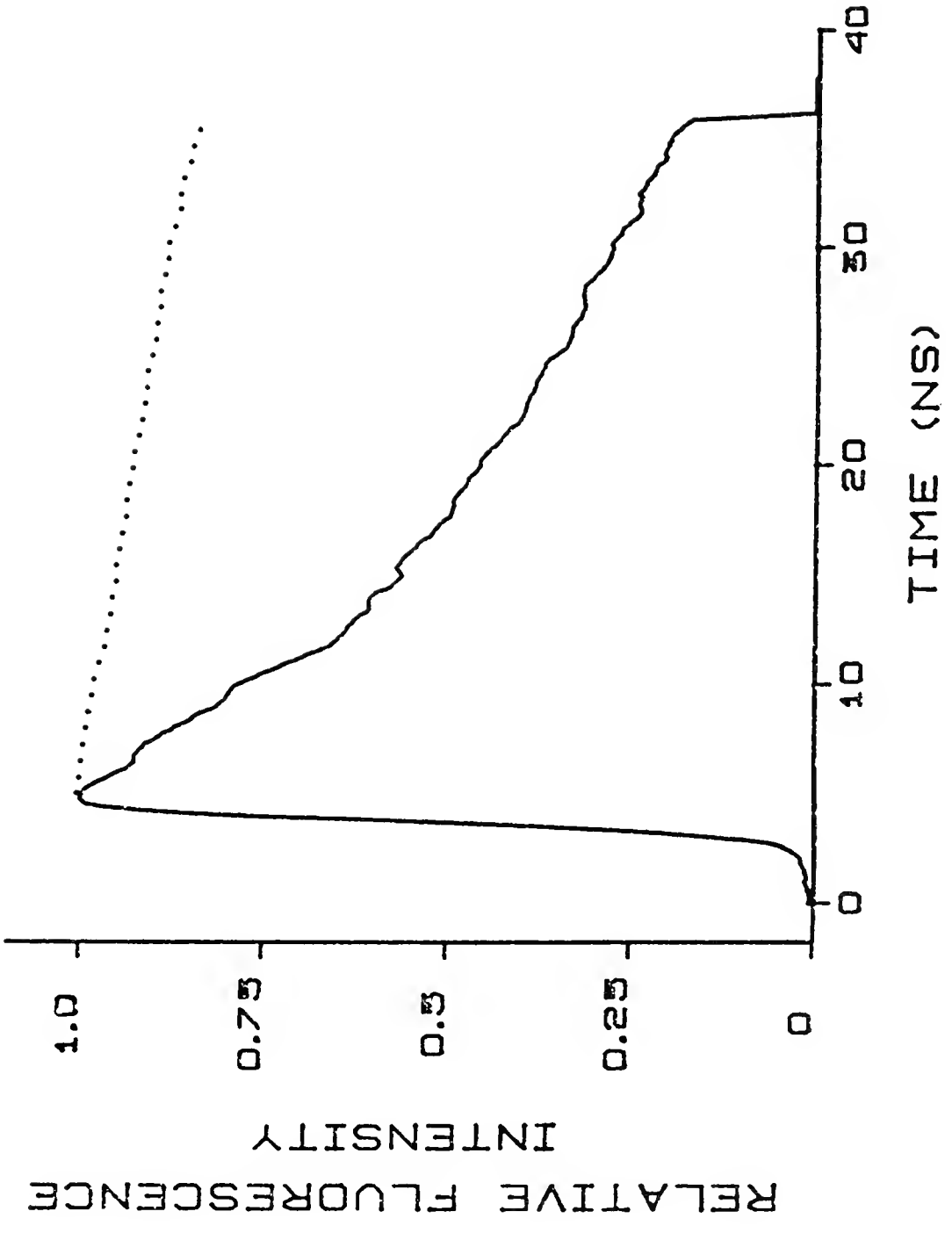
RELATIVE FLUORESCENCE INTENSITY
1.0
0.75
0.5
0.25
0
0
10
20
30
40
TIME (NS)

pumped by the N_2 laser. The actual mechanics of this laser, the pulse widths and wavelengths obtained are reported in the next chapter. The point of interest here is that pulses on the order of 200 to 400 ps were obtained, emitting over a broad band, with relatively good output power. The first attempt at frequency doubling this output failed to produce observable UV lasing. However, further modifications are planned and the attempt will be made again.

The dye laser output, using DPS dye, was used to excite perylene. The lifetime measured was comparable to that measured with the N_2 laser. Also, a mixture of perylene and quinine sulfate in ethanol was excited with the DPS dys laser and the intensity decay curve resulted in the measurement of the lifetime of perylene. Hence, only the perylene was excited by the DPS lasing, allowing for an effective means of measuring the perylene lifetime by selective excitation. When the mixture was excited by the N_2 laser, the intensity decay obtained was a mixture of both decays from perylene and quinine sulfate, as discussed below. Since the dye laser output was lower in power than the N_2 laser and observable UV lasing was not obtained, for the remainder of this work, the N_2 laser was used as the excitation source.

Limits of Detection

The entrance coupling optics used for the temporal disperser were specified only for the visible region of the

spectrum. Fluorescence below ~400 nm was not observable. The N_2 laser itself was not observable through these optics either, so scatter from the laser was not important. In fact, the temporal disperser was quite insensitive overall. In Table VIII, limits of detection and linear dynamic ranges obtained for a few compounds using the finder mode and the normal streaking mode are listed. For most of the temporal measurements made in this section, signal levels giving reasonable S/N for the streak camera resulted in PM saturation for the PM-boxcar system.

In the determination of the limits of detection, two points should be made. In the finder mode, with the trigger delay set such that the temporal information is compressed at the top of the streak, jitter and drift have very little effect. Hence, the peak intensity always occurred in one of two channels. The limiting noise was taken to be the standard deviation of sixteen measurements of the blank in these two channels.

In the normal streak mode, when the temporal disperser is set to the shortest time range, the jitter and drift for the system became an important problem. Also, at low signal-to-noise ratios, the step seek computer search routine broke down and was useless. Hence, the data were averaged as presented with no corrections for jitter or drift. In this case, limiting noise had to take into account the variations across the entire temporal disperser output. This was done by averaging the peak to peak variations for sixteen blank

Table VIII. Streak Camera Limits of Detection and Linear Dynamic Range.

Compound	Finder Mode LOD(ppb)	Finder Mode LDR	Normal Streak Mode LOD(ppb)	Normal Streak Mode LDR
quinine HCl	0.8	0.0008-10 ppm	100	0.1-10 ppm
7,8-benzoflavone	9	0.1-30 ppm	100	0.1-30 ppm
anthracene	1	0.3-10 ppm	100	0.1-10 ppm
riboflavin	2	0.002-10 ppm	200	0.2-10 ppm

measurements and multiplying this by three fifths. This gives a conservative estimate of the limit of detection. However, if only ten channels were used, instead of all 256, the LOD would only drop by a factor of three.

Mixtures

Temporal measurements were made on three binary mixtures of compounds. In each case, the pure compounds were measured first and then the mixture. The mixtures were made by adding equal volumes of solutions of the two compounds being used, at concentrations that gave approximately equal peak intensities when the compounds were determined separately.

The first mixture tested was perylene and quinine sulfate in ethanol at 445 nm. For the pure components, the measured lifetimes of perylene was 5.7 ns and of quinine sulfate was 18.7 ns. In the approximately equal intensity mixture, 14 ppm perylene and 12 ppm quinine sulfate, the decay obtained yielded only one lifetime, 6.5 ns; it was not possible to deconvolute the decay curve for the longer lived component. The concentration of the quinine sulfate was increased, giving a mixture of 15 ppm perylene and 130 ppm quinine sulfate. Again the measured decay yielded only one lifetime, 14.0 ns. The monochromator wavelength was changed to 470 nm and this higher concentration mixture ran again. The lifetime measured was 13.8 ns. At this wavelength, only the emission from the perylene is being observed.

The final mixture ran, using these two compounds, was 12 ppm perylene and 200 ppm quinine sulfate at 470 nm. This mixture also gave only one lifetime, 17.8 ns.

From these results, it is clear that the perylene was absorbing the emission from the quinine sulfate and re-emitting the absorbed energy at its characteristic fluorescence wavelength. In fact, the perylene absorption band does overlap the fluorescence band for quinine sulfate. Hence, for time resolution to work, another condition must also be met. The absorption band of the shorter lifetime component can not overlap significantly with the fluorescence band of the longer lifetime component.

The second mixture used was anthracene (τ = 4.7 ns) and 1,2,5,6-dibenzanthracene (τ = 13.0 ns), two more closely related compounds. The approximately equal intensity mixture was 15 ppm of both in ethanol, monitored at 417 nm. A single lifetime value was again obtained, 5.6 ns. The mixture was changed to 15 ppm anthracene and 30 ppm 1,2,5,6-dibenzanthracene, and a longer lifetime component was made visible. The measured lifetimes were 5.6 ns and 10.3 ns. On changing the concentrations to 10 ppm anthracene and 30 ppm 1,2,5,6-dibenzanthracene, the two lifetimes were measured as 6.2 ns and 10.4 ns. In both cases, the correlation coefficient obtained from the least squares of the longer lifetime component was poorer than that obtained for the faster component. Since the fluorescence and absorption

bands do not overlap significantly for these two compounds, the absorption-re-emission process was most likely not occurring.

The anthracene-1,2,5,6-dibenzanthracene mixture was repeated in n-heptane. With 1 ppm anthracene (τ = 3.0 ns) and 10 ppm 1,2,5,6-dibenzathracene (τ = 8.5 ns), a single component lifetime of 5.5 ns was measured. These lifetimes are too similar, in this mixture, to be temporally separated with the present system without further deconvolution.

The last mixture reported here is that of 9 ppm cephradine (τ = 1.4 ns) and 23 ppm quinine sulfate (τ = 18.7 ns) in ethanol, with the emission monochromator set to a wavelength reading of 000; this allows the zeroth order to be passed straight through the monochromator with no dispersion. In this case, a fast lifetime component was distinguishable from a longer lifetime decay. The two lifetimes measured were 3.3 ns and 8.3 ns for 100 shots averaged. When 1000 shots were averaged these two components were determined to be 3.5 ns and 15.6 ns, Figure 21. This indicates that the S/N for an average of 100 shots is not adequate for mixture analysis where the trailing edge of the decay curve is needed to make the determination. A thousand shots is a definite improvement, but still not enough to reproduce the correct lifetime. Also, with deconvolution, a better estimate of the fast lifetime component should be possible.

Figure 21. Cephradine-Quinine Sulfate Mixture Fluorescence

(——) Linear fluorescence signal
(···) Natural logarithm of fluorescence signal

Obtained with Streak Camera System

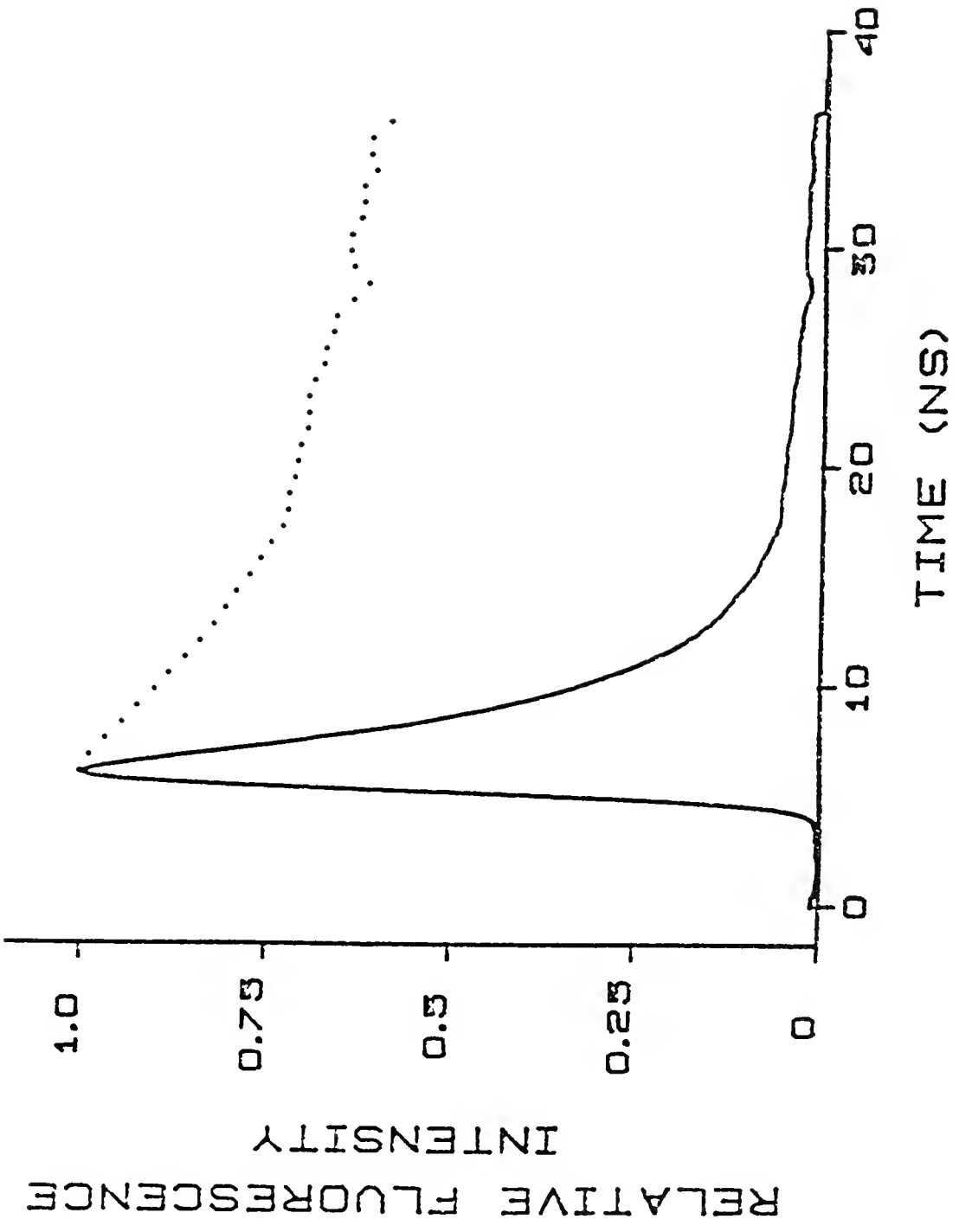
RELATIVE FLUORESCENCE INTENSITY
1.0
0.75
0.5
0.25
0
0
10
20
30
40
TIME (NS)

An interesting observation was noted for rubrene. When excited by the N_2 laser, two fluorescence bands are observed spectrally, one with a maximum at 556 nm, the other at 415 nm. Temporally, the 556 nm component has a lifetime of 11.2 ns, in n-heptane, while the 415 nm component has a lifetime of 2.8 ns. The fluorescence at 415 nm has been attributed to impurities (108). Hence, temporal information can be used to support spectral data.

External Heavy Atom

From the lifetimes given in Table VII, the general trend is with increasing external heavy atom concentrations, the fluorescence lifetime decreases, with iodide having a larger effect than silver. However, for riboflavin, the lifetimes appears to increase slightly at the lower concentrations of the heavy atom perturber. The reason for this is unclear. The same trend appears to be observable in several other cases, but these are within experimental error.

At the higher concentration of heavy atom perturber, the observed fluorescence lifetime is definitely reduced. There appears to be a threshold concentration at which the effect takes place. A similar observation was made for phosphorescence lifetimes (4,31). These results conform with the idea of increased intersystem crossing from the excited state singlet, to the excited state triplet, and increased non-radiative decay from the excited state triplet to the ground state singlet.

Methods Comparison

In Table IX, a comparison of the more popular fluorescence lifetime determining techniques available today is given. Only the time-correlated signal-photon counting (TCSP) and phase shift techniques represent complete systems, sold as such from the manufacturers. All other systems require an excitation source, monochromator, and detector (except for the streak camera which has an integral detector).

For temporal measurements using a pulsed source, a synchronously pumped, mode locked, cavity dumped dye laser would offer the closest approximation to a delta function excitation source. However, such commercial systems sell for ∿$70 k. Also, only the streak camera or TCSP systems could take full advantage of the short pulses produced to extend their temporal analysis ranges. As a result, other excitation sources could be more appropriate, such as pulsed lasers, cavity dumped CW lasers, or flashlamps. The cheapest of these are the flashlamps, ∿$5k; however the pulse widths are considerably longer, 2 to 20 ns.

Monochromators equivalent to those in the complete systems would cost from $1500 to $3000. Equivalent PM's could be purchased for approximately $500. However, these photomultiplier tubes would have a rise time of about 2 ns, further limiting the temporal working range of the technique. Static cross field photomultipliers are available commerically, at a cost of ∿$8k, with a rise time of ∿100 ps.

Table IX. Comparison of Fluorescence Lifetime Measurement Systems.

Technique	Detector	Temporal[c] Resolution	Lifetime Range[d] Measurable	Sensitivity
Sampling oscilloscope/ Boxcar	1) SCFP[a]	25 ps - 1 ns	500 ps - 10 μs	moderate
	2) PM [b]	25 ps - 1 ns	2 ns - 10 μs	excellent
1 GHz real time oscilloscope	1) SCFP	350 ps	1 ns - 10 μs	moderate
	2) PM	350 ps	2 ns - 10 μs	excellent
Transient digitizer	1) SCFP	350 ps	1 ns - 10 μs	moderate
	2) PM	350 ps	2 ns - 10 μs	excellent
Streak Camera	-	<1% of full scale range (10 ps)	50 ps - 100 ns	moderate
+ vidicon and analyzer	-	"	50 ps - 100 ns	moderate
TCSP	SCFP	20 ps	100 ps - 10 μs	moderate
Complete systems				
TCSP	PM	100 ps	500 ps - 10 μs	excellent
Phase shift	PM	100 ps	500 ps - 10 μs	excellent

(a) SCFP - static cross-field photomultiplier

(b) Common photomultiplier

(c) Limited by electronics

(d) Limited by detector and fluorescence lifetime

Table IX - extended.

Relative analysis time	Directly Quantitative	Detection system cost
slow	yes	$20k
slow	yes	$12k
fast	yes	$30k
fast	yes	$22k
fast	yes	$40k
fast	yes	$32k
fast	yes	$40k
fast	yes	$70k
slow	no	$30k
slow	no	$44k
moderate	yes	$34k

Unfortunately, the signal gain is limited to about 10^4. The trade off for higher gain is slower speed.

Also not included in the comparison, are user programmable computers. In every case, a computer would make the system more versatile. The more expensive streak camera system had a microcomputer analyzing system that performs approximately the same function as a multichannel analyzer (MCA) for the TCSP.

The conclusion that can be drawn from the information in Table IX is that the greater the temporal resolution, the larger the signals must be, and the higher the cost of the instrumentation. All of these factors must be weighed against the task being worked on and what type of information is needed.

If fluorescent species with small signals, and relatively long lifetimes are to be observed, then the PM-boxcar system is adequate, noting that the analysis time is long. For temporal measurements in the 100 ps to 1 ns range, the streak camera or TCSP systems are the valid choices. To directly measure laser pulses in this range, the streak camera is the best choice.

The instrumentation cost in being able to obtain temporal information with an order of magnitude greater resolution or time range on a per pulse basis, increases by a factor of four. However, a point of realization is that the higher temporal resolution systems, the streak camera,

for example, offer more information with a shorter pulse width excitation source. Hence, more expense for a more versatile system.

CHAPTER IV
SUBNANOSECOND PULSED DYE LASER

Introduction

In molecular spectroscopy, the generation of subnanosecond, spectrally broadband laser pulses can be of considerable importance, as mentioned previously. The spectral broadband output is also useful in that more optical power can be pumped into the molecules of interest because of their broadband absorption. In the recent past, picosecond pulses have been generated by mode locking of various dye lasers (109-118). These types of lasers are now commerically available, although the cost is still quite high. There has also been reported the production of subnanosecond dye laser pulses by passively mode locking a dye laser pumped by an N_2 laser (119). Another N_2 laser pumped dye laser system has been used to generate subnanosecond pulses by making use of resonator transients (120). In each case, broadband output could have been obtained if the spectral tuning element in each case would have been replaced by a nontuning element, i.e., if a mirror had replaced the grating in most cases.

Presented here is a simple inexpensive design for the generation of subnanosecond, broadband pulses from an N_2 pumped dye laser. The once critical alignment necessary for

most dye laser systems is minimized to the extent that the entire dye laser is self-contained. The design is an improvement on the one reported by Capelle and Phillips (121) or as suggested by Schafer (122).

Dye Laser Design

The N_2 pump laser was a Garching Instruments Type SP 1/2 TEA N_2 laser (available through Interactive Radiation, Inc., Northvale, NJ). The output was approximately 20 kW peak power with a 1.0 ns pulse width (FWHM). The dye laser itself was simply a 1 cm square fluorescence cell, of which, one side was coated with aluminum by vacuum plating. The laser cavity was defined by the totally reflecting back mirror and the uncoated quartz cell window (approximately 6% reflectivity). The dye laser is transversely pumped by a N_2 laser, coupled by the use of a cylindrical lens (focal length = 3 cm). A small stirring bar was used to stir the dye solution. In Figure 22, a schematic diagram of the N_2 laser pumped dye laser is given.

The optical output power was measured with an ITT F4000 biplanar vacuum photodiode, rise time $\leq$ 500 ps (ITT, Fort Wayne, IN) and a Tektronix 1S1 sampling head, rise time $\leq$ 350 ps (Tektronix, Inc., Beaverton, OR). The spectral output was measured by passing the emission through an ISA H-10 0.1 m monochromator (ISA, Metuchen, NJ) and measuring the output with a Hamamatsu R777 photomultiplier (Hamamatsu,

Figure 22. Block Diagram of TEA N_2 Laser Pumped Dye Laser for Subnanosecond Excitation Pulses

(A) TEA N_2 laser
(B) Cylindrical lens
(C) Dye laser
(D) Sample cell
(E) Detection system
(M) Mirrored surface

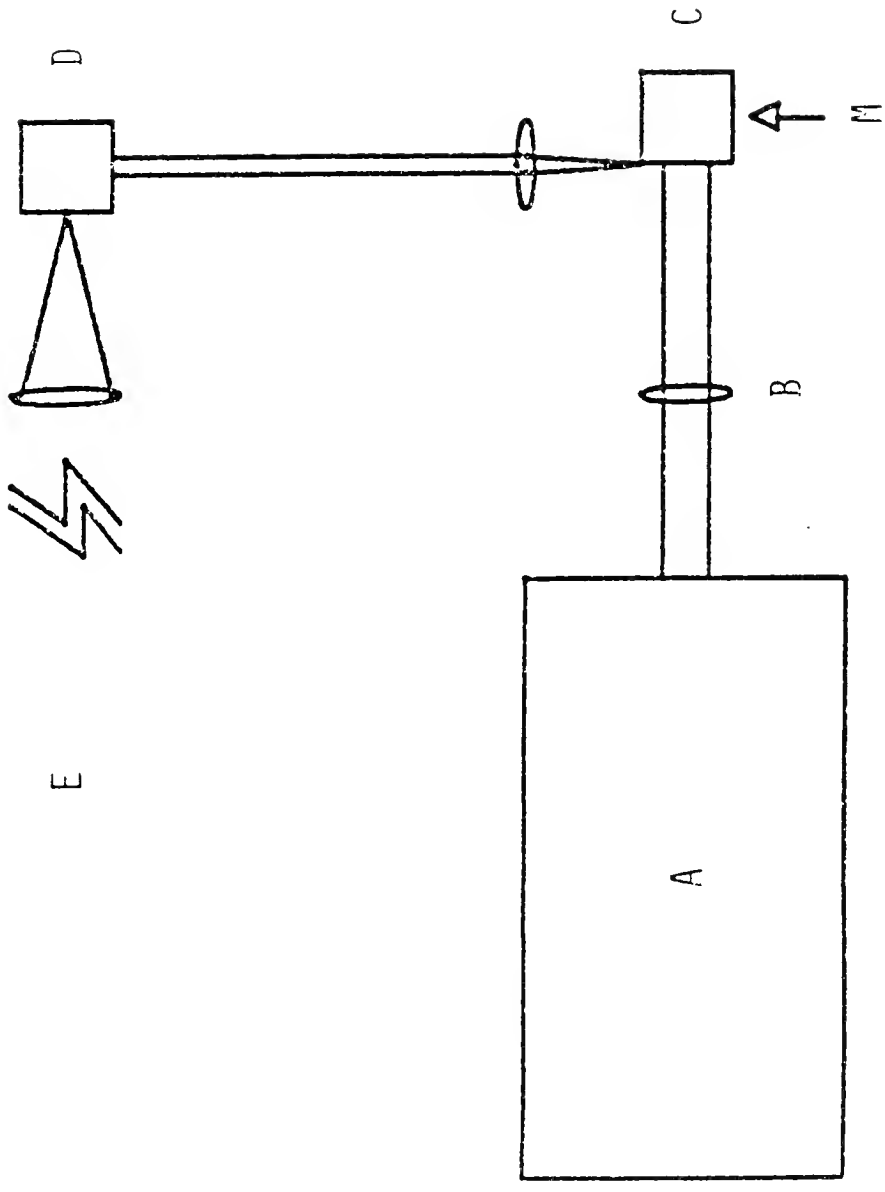
D
C
M
B
E
A

Middlesex, NJ). The signal current was monitored by an EG&G, Princeton Applied Research boxcar averager, 163-164 combination with a Tektronix S-2 sampling head (EG&G, PARC, Princeton, NJ). The pulse width measurements were made using Hamamatsu temporal disperser system consisting of the temporal disperser (Model C979) with slow plug-in module (Model M1284), vidicon camera and controller (Model C1000-12) and temporal analyzer (Model C1098).

Results and Discussions

The results obtained with several dyes are given in Table X, the powers listed are relative to the N_2 pump laser. The divergence of the dye laser beam is about 10 milliradians for the overall optical output, lasing and superirradiance. The laser beam along has a divergence of approximately 3 milliradians. The overall beam quality was significantly improved by placing an f/5 lens one focal length away from the dye laser. This lens did not actually couple with the dye cell cavity, because the production of the laser output was constant with lens x,y,θ positioning while peak power and pulse width essentially remained the same.

As has been pointed out previously (120), the dyes having longer fluorescence lifetimes actually give shorter pulse widths. It is also of interest that the overall efficiency of the dye laser is quite good (as high as 20% of the optical input power from the N_2 laser is emitted from the dye

Table X. Dye Laser Relative Outputs.

Dye Laser	Wavelength Peak (nm)	Wavelength Range (nm) (10% points)	Relative Peak Power[a,b]	Pulse Width (ns)[c]	Relative Average Power
DPS Dye	405	395 - 415	0.5	0.38	0.2
7D4MC Dye	455	439 - 471	0.5	0.22	0.1
7D4TMC Dye	481	465 - 497	0.3	0.26	0.1
R6G Dye	586	576 - 596	0.4	0.22[d]	0.1

(a) 18 Hz repetition rate.

(b) All powers taken with respect to N_2 laser being unity. N_2 laser has a 1.0 ns pulse width and an energy of 20 μJ/pulse. Note that the output on the photodiode was rise time limited.

(c) Single pulse measurement.

(d) Laser Precision radiant power meter gave value of 1.8 μJ/pulse.

laser). A similar efficiency has been reported by Fan and Gastafson (117). In comparison with other systems, this seems rather large, but it should be noted that this is broadband emission over several nanometers instead of approximately one angstrom for more typical dye lasers.

Since the dye laser is entirely self-contained, there is no need for highly reproducible optical mounts. In fact, the first attempts at getting the dyes to lase were performed by the experimenter actually holding the cylindrical coupling lens and dye laser by hand to perform the optical adjustments. At this time, it takes less than five minutes to change dyes and "re-align" the entire system. The use of several cells would cut this time down to less than a minute.

The results reported here were all obtained for an 18 Hz repetition rate with vigorous stirring. Above 35 Hz, the output dropped significantly. A future improvement consists of a flow through cell which should allow higher repetition rates. Another improvement, to add to the versatility of the dye laser, is to use an etalon to replace the back mirror. This would give a narrower spectral bandwidth and even add tunability to the system. Finally, various attempts are being made to further decrease the temporal pulse width of the dye laser.

CHAPTER V
SUMMARY AND FUTURE WORK

Noise power spectra for an inductively coupled argon plasma were determined under various conditions. The major noise components observed were white noise, low frequency noise, and proportional noise. Quantitative results for these noise components are given. The proportional noise observed increased with concentration of analyte, RF power, decrease in coolant gas flow rate and decrease in nebulizer flow rate. The DC signal followed the same trend. Increasing the observation wavelength increased the observed frequency at which the low frequency component reached 10% of its maximum amplitude. Changing the observation height in the plasma, with yttrium being aspirated, determined which noise components were visible in the power spectrum. At observation heights near the power coils, all three noise components were present, whereas, at a significantly greater height, the low frequency noise dominated. Changing the torch design changed the relative amplitudes of the different noise components but did not greatly change the frequencies at which they occurred. Changing the drain tube length or cavity volume had little effect on the noise power spectra.

For the spectral noise power analysis of the ICP, several points could be elaborated on. An improved anti-aliasing filter should be used to eliminate the fold-over problem encountered. The low frequency components should be examined more thoroughly since this is the region that is most often used in monitoring the emission signals from the ICP. Also, the anti-aliasing filter would be a necessity for this study. An improved amplifier, or the use of batteries with the existing amplifier, should be used to minimize the 60 Hz components coming from this source. Also, a 60 Hz notch filter could be used to get rid of this 60 Hz problem.

Another use of the noise power analysis of the ICP would be to determine the spectra of the OH (∿306 nm) band to give a better indication of the contribution due to water alone. An element near the OH band, such as copper (λ = 324.7 nm), should also be run to indicate more optimal frequencies for modulation. Of great interest would be a brief study to determine the relationship of the amplitude of the proportional noise components observed at ∿210 Hz with concentration. This could easily be done with a wide band AC amplifier and a bridge to give a DC output.

Other areas of interest for the power spectra measurements are for analytical excitation sources, such as inert gas arc discharge lamps, and flames. The use of the power spectra, or the correlogram, to locate noise sources should definitely be considered.

Also reported is the temporal measurement of fluorescence signals using two different pulse measurement techniques. The first measurement technique discussed is a PM-boxcar approach. The second is a streak camera system. Although the PM-boxcar system is more sensitive, it suffered from poor overall temporal resolution due to trigger jitter and PM temporal response. The streak camera approach is by far the best, in terms of temporal information, however, the signal levels needed for its operation are relatively large. The streak camera was used to determine external heavy atom effects on fluorescence lifetimes and an attempt was made to recover the fluorescence lifetimes of two spectrally overlapping fluorescent compounds in a mixture.

For the temporal fluorescence measurements several ideas can be tested, the most important of which involves the streak camera. A correlation function could be used to sort out bad temporal information on a shot-to-shot basis. Correlation could also be used to determine how to average the information from various shots. A correction could be made for the change in laser pulse intensity per shot by splitting off part of the beam and monitoring it with a photodiode. Instead of the 256 point resolution of the TA, connecting the SIT controller directly to the minicomputer could give up to 1024 points of resolution. To speed up the data transfer, the direct memory access (DMA) could be used. This would also allow three dimensional analysis per streak. A video tape could be used as a means of storing this large amount of information.

A change in the FORTRAN programming that would improve the temporal resolution is to set up a "look-up" table based on the actual time interval per channel of the SIT instead of a linear approximation. A trivial change in design would be to use a smaller sample volume. In most cases, the larger sample volume is not needed and this would allow for a smaller time spread in the fluorescence signal being passed to the streak camera. This last point is important only if temporal information on the order of 50-100 ps is to be obtained. A design change for the streak camera would be to replace the entrance coupling optics with mirrors instead of lenses.

The measurement of atomic lifetimes in a flame, or other atom cell, would be of interest. If the proper excitation source is used, important information about flame kinetics and atomic kinetics in a flame could be obtained.

For the dye laser system, shorter pulses might be obtained by shortening the cavity length. Also, a shorter pumping pulse, for example, from a high pressure N_2 laser, would be of interest. Setting up an etalon with a partially mirrored rear cell wall and a 100% mirror would allow narrow band lasing and tunability of the output. Both of these improvements could also lead to a high enough peak intensity for efficient frequency doubling to obtain UV excitation pulses of tens of picoseconds in duration.

As always, the beginning of one project leads to several more. Such is the case of this work. The extension here would be to obtain a three dimensional temporal scan, four dimensions in total. These dimensions would be time, excitation wavelength, emission wavelength, and intensity. The instrumentation needed to obtain this information is available presently. A simple approach would be to use the multiple window streak camera, available from Hamamatsu, to obtain time, emission wavelength, and intensity on the picosecond scale. The excitation pulses would come from a technique known as continuum generation (123,124). A high power mode locked laser is focused into water, producing a continuum of light extending from the near IR to the UV, on the picosecond time scale. An excitation monochromator could be scanned to give the change in excitation wavelength.

Unfortunately, this approach does not give a four dimensional output per pulse. However, the basic tools are available today; their application is all that is needed.

APPENDIX A
FORTRAN PROGRAM USED FOR ICP DATA REDUCTION

The FORTRAN program, called DSP, used to collect the data (see Appendix B), obtain the power spectrum, and return the results, is given here. All programs presented in these appendices were designed to run on a Digital Equipment Corp. (DEC) PDP 11/34 minicomputer under the RT-11 operating system. The programs described here and in Appendix C were written in FORTRAN IV, supplied by DEC, and the programs discussed in appendices B and D were written in assembly language.

In Figure 23, the flow chart for the program DSP is given. The program can be used for collecting and interpreting new data or re-evaluating previously determined power spectra. If the re-evaluation was chosen, the filename of the old power spectrum was used to recall the information stored on disk and the number of data points and sampling rate used to collect the original data was used to determine the corresponding frequency scale. The re-evaluation allowed certian frequency components to be set to zero. This permitted an expansion of the amplitude of the power spectrum being displayed by setting the value of the component with the largest amplitude to zero. This was how the zeroth harmonic was eliminated.

Figure 23. Flow Chart for FORTRAN Program Used for ICP Noise Power Study

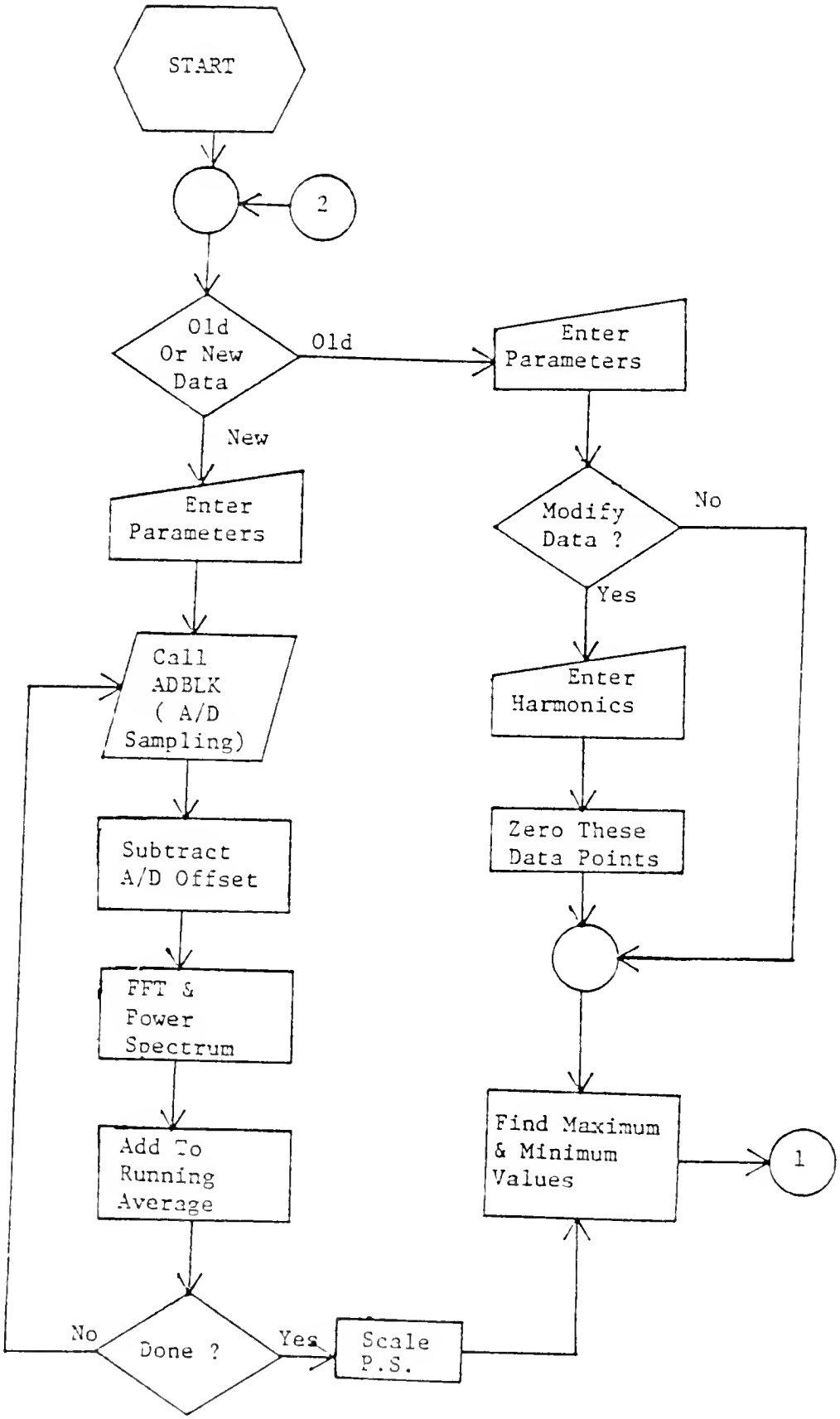
START
2
Old Or New Data
Old
Enter Parameters
New
Enter Parameters
Modify Data ?
No
Yes
Enter Harmonics
Zero These Data Points
Call ADBLK (A/D Sampling)
Subtract A/D Offset
FFT & Power Spectrum
Add To Running Average
Done ?
No
Yes
Scale P.S.
Find Maximum & Minimum Values
1

Figure 23 - continued

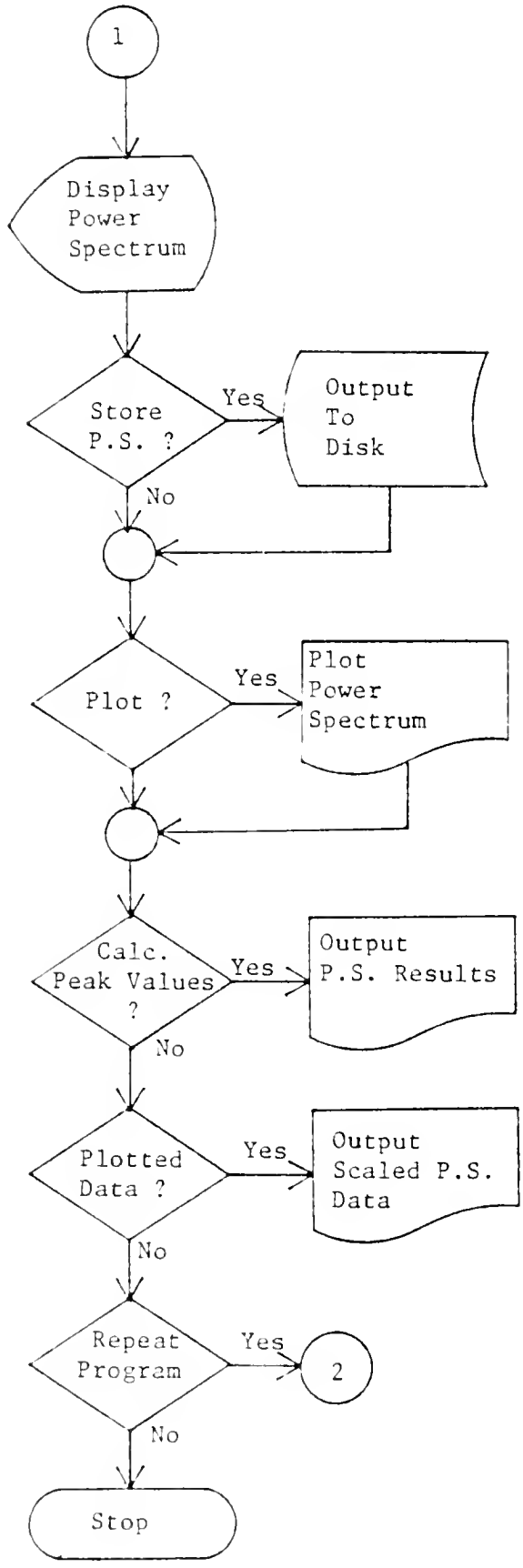
1
Display Power Spectrum
Store P.S. ?
Yes
Output To Disk
No
Plot ?
Yes
Plot Power Spectrum
Calc. Peak Values ?
Yes
Output P.S. Results
No
Plotted Data ?
Yes
Output Scaled P.S. Data
No
Repeat Program
Yes
2
No
Stop

If new data were to be collected, the operating parameters were entered, i.e., number of points per data set, number of power spectra to average, sampling rate, A/D channel and amplifier gain (including load resistor). A loop was then entered which acquired the data (Appendix B), obtained the FFT and power spectrum, and kept a running average of the power spectra determined. This loop terminated after the correct number of spectra were averaged, and this averaged spectrum scaled by the amplifier gain.

At this point, the new power spectra and the old power spectra were treated the same. The maximum and minimum amplitudes were found and these values printed at the terminal. The power spectrum was scaled using the maximum amplitude value and the maximum D/A value allowed (4095), and the results displayed on an oscilloscope. If the power spectrum was to be saved, the information was stored on disk. If a plot was desired, the scaled power spectrum being displayed on the oscilloscope was output to an analog plotter through the D/A's.

The amplitude and frequency information was also determined for a maximum of 100 values with the largest amplitudes. The average of the remaining data was calculated, along with the standard deviation and all of this information printed out at the terminal. The plotted data was also available to be printed on the terminal if desired.

The sampling routine for the A/D is discussed in Appendix B. The FFT and power spectrum routine, as well as the display routines, were obtained from DEC. The plotting

routine used an assembly language routine to drive the D/As written by Dave Bolton.

APPENDIX B
ASSEMBLY LANGUAGE PROGRAM FOR THE FAST SAMPLING OF ONE CHANNEL OF THE LPS-11

This assembly language program, called ADBLK, was written specifically for high speed A/D sampling using the DEC LPS-11 under the RT-11 operating system. Only one channel is sampled and an entire data array is filled upon calling this subroutine. The maximum sampling rate used for this work was 25 kHz, however faster rates were possible. The flow chart for the routine is given in Figure 24.

At the entry point of the routine, the computer registers were stored and the parameter list read in, i.e., the data buffer to be used, the number of data points to be sampled, the rate at which the data was to be taken, and the channel to be used. Then an interrupt service routine was enabled to allow the A/D to be sampled. The interrupt routine sets up the operating parameters for the A/D and timing clock, and initializes a counter. When the clock overflows, the A/D is sampled, the data stored, and the counter decremented. This cycle is repeated until the counter reaches zero, then the computer registers are restored to their previous values and control returned to the FORTRAN program.

Figure 24. Flow Chart for Assembly Language Program for A/D Sampling

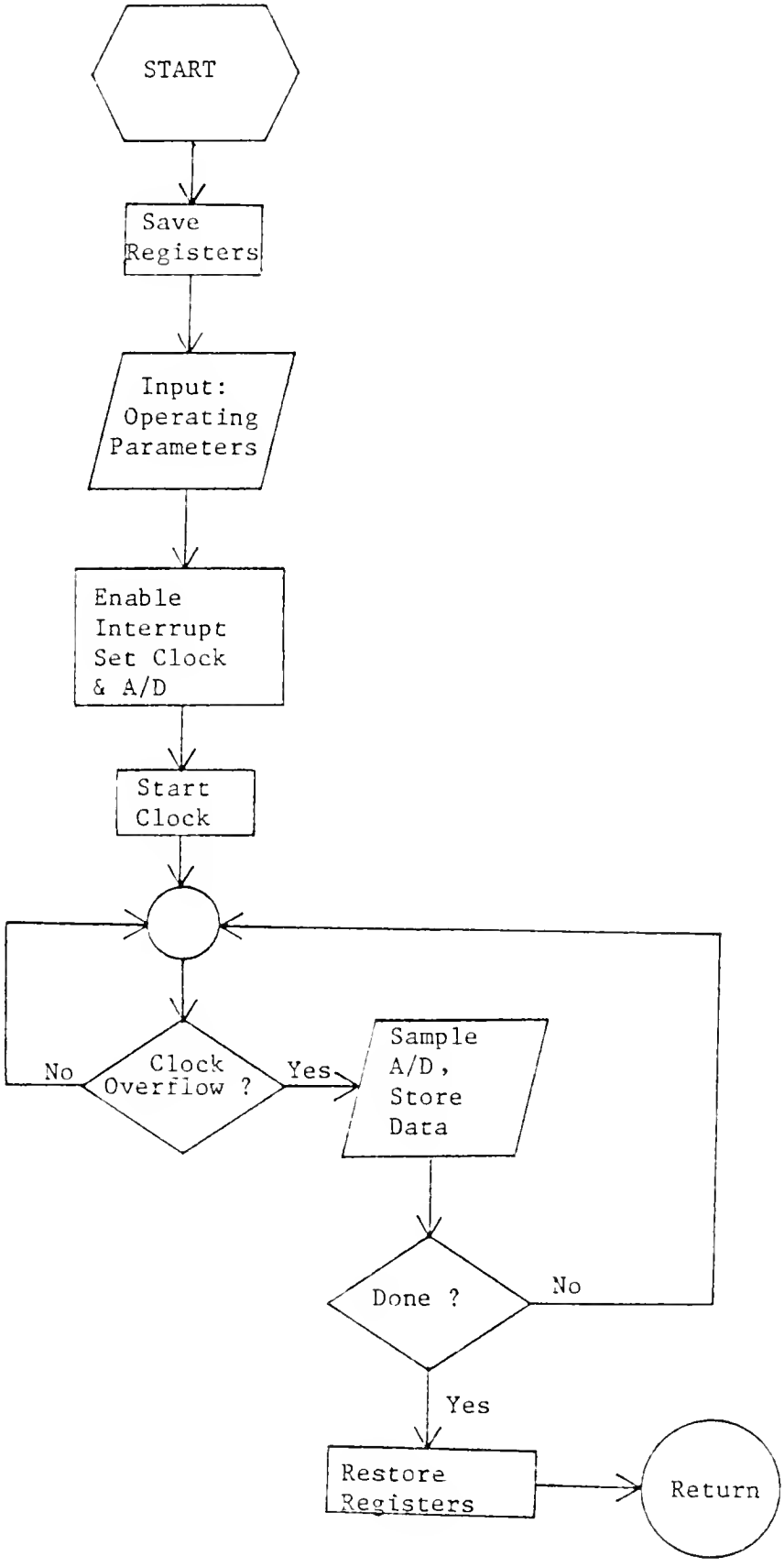
START
Save Registers
Input: Operating Parameters
Enable Interrupt Set Clock & A/D
Start Clock
Clock Overflow ?
No
Yes
Sample A/D, Store Data
Done ?
No
Yes
Restore Registers
Return

To enter the interrupt service routine the first time, the A/D was set to interrupt on a clock overflow and the clock started. A dummy loop was used to hold the computer until the interrupt occurred. In the interrupt service routine, this first A/D sampling had to be cleared or an error occurred. The A/D interrupt routine used a loop when waiting for the clock to overflow between data samplings.

APPENDIX C
FORTRAN PROGRAM USED FOR DATA TRANSFER FROM THE TEMPORAL ANALYZER AND FOR FLUORESCENCE LIFETIME DETERMINATION

The program described here was for the calculation of single fluorescence lifetimes from temporal fluorescence intensity decay signals. The data were acquired by the Hamamatsu streak camera system described previously, and transferred, under program control, to the DEC PDP 11/34. The name of the program was STST, and a flow chart for this program is given in Figure 25.

As with the FORTRAN program DSP (Appendix A), STST could be used to look at old or new data. If old data were chosen, the data collection section of the program was omitted and the remainder of the program was used. The operating parameters needed were time range covered by the streak camera, and the number of data sets averaged. From the time range information, a value was calculated for the time interval per channel. A provision was made for the subtraction of a dark current file, however, for this work the dark current subtraction was performed by the Temporal Analyzer (TA) prior to data transfer.

Figure 25. Flow Chart for FORTRAN Program for Data Transfer and Fluorescence Lifetime Determinations Using Streak Camera System

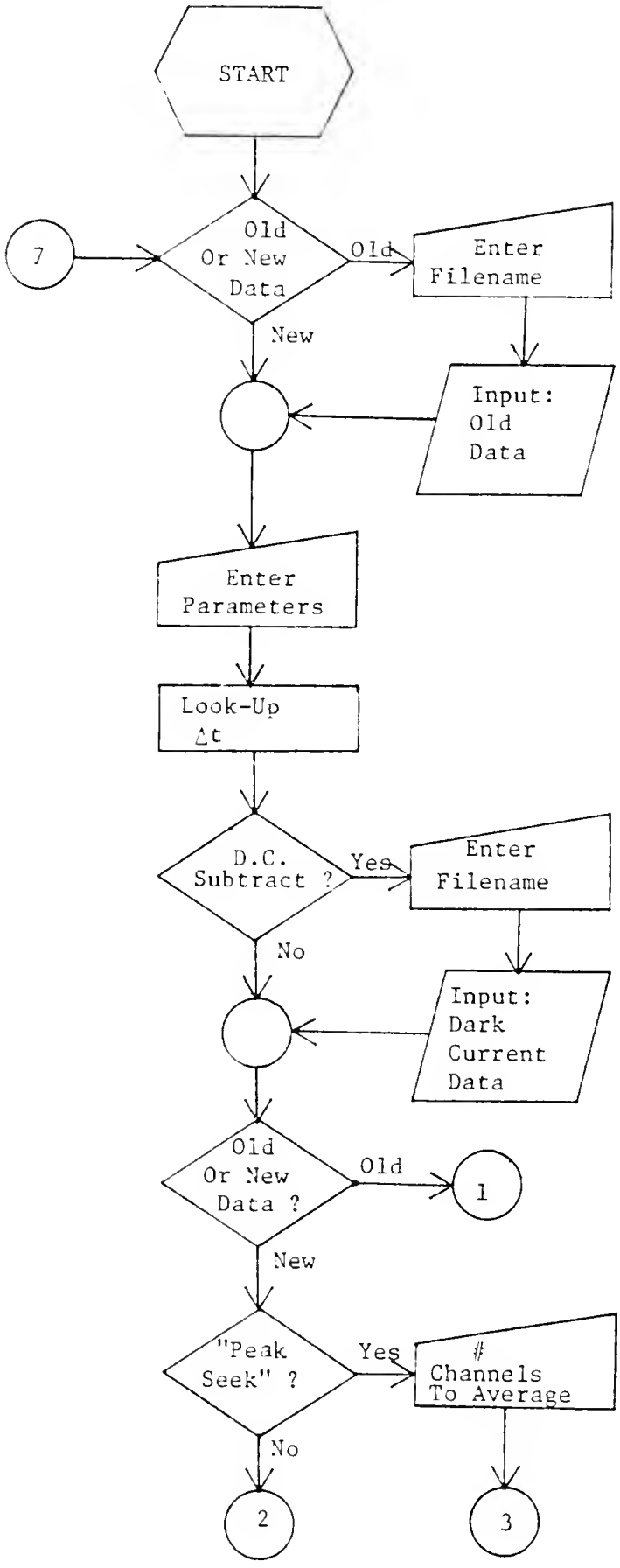
START
7
Old Or New Data
Old
Enter Filename
New
Input: Old Data
Enter Parameters
Look-Up Δt
D.C. Subtract ?
Yes
Enter Filename
No
Input: Dark Current Data
Old Or New Data ?
Old
1
New
"Peak Seek" ?
Yes
Channels To Average
No
2
3

Figure 25 - continued

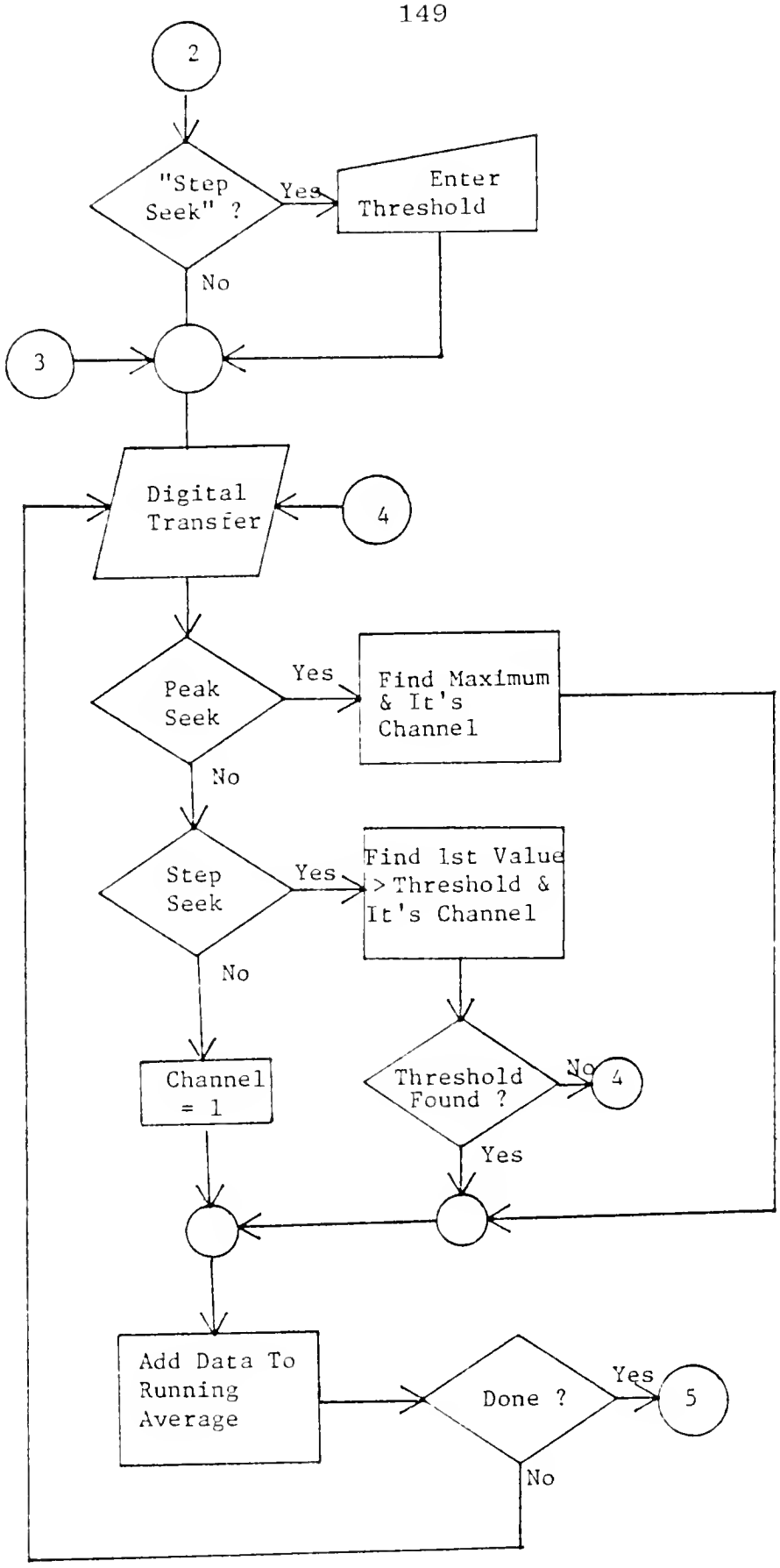
2
"Step Seek" ?
Yes
Enter Threshold
No
3
Digital Transfer
4
Peak Seek
Yes
Find Maximum & It's Channel
No
Step Seek
Yes
Find 1st Value > Threshold & It's Channel
No
Channel = 1
Threshold Found ?
No
4
Yes
Add Data To Running Average
Done ?
Yes
5
No

Figure 25 - continued

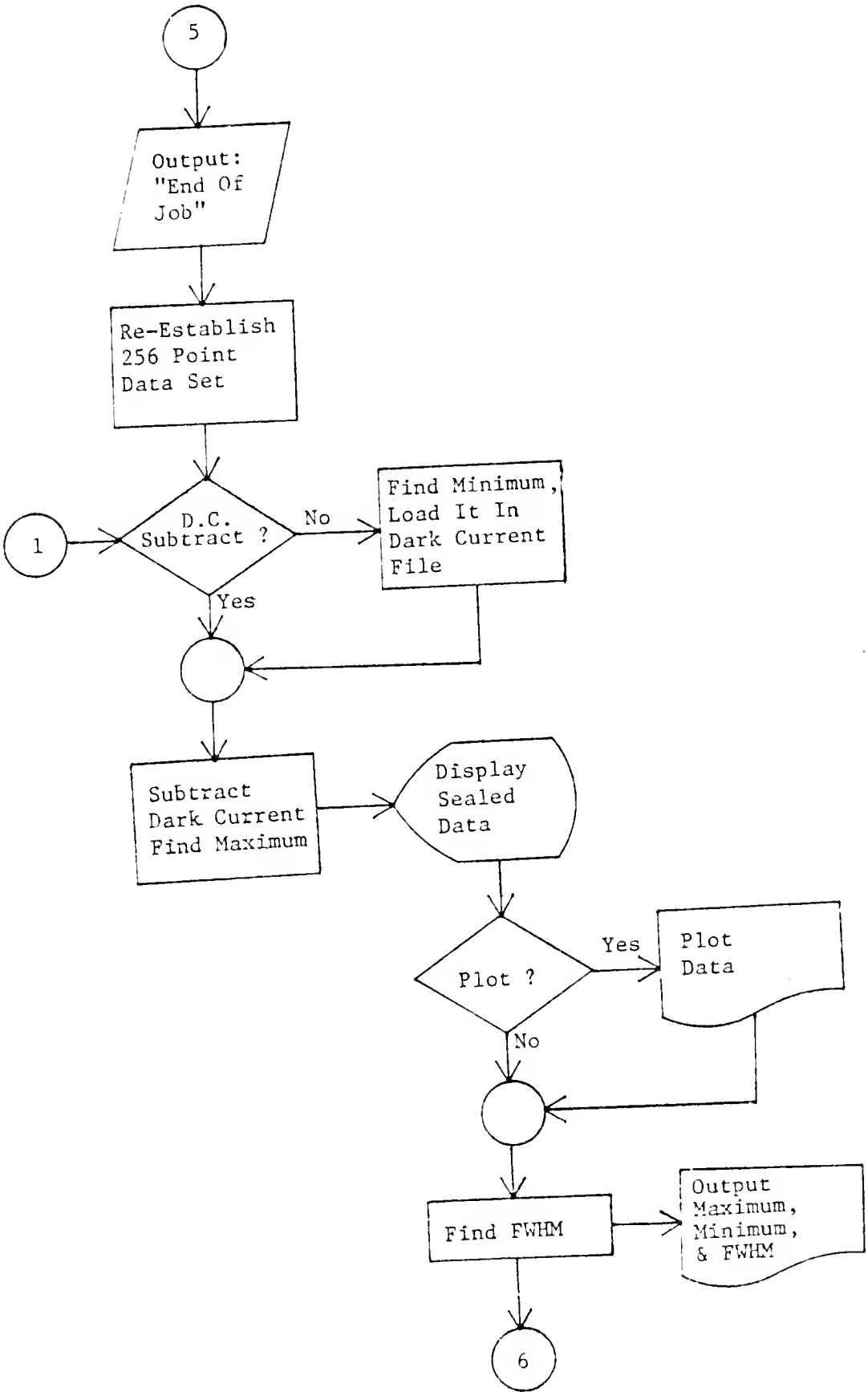
5
Output: "End Of Job"
Re-Establish 256 Point Data Set
1
D.C. Subtract ?
No
Find Minimum, Load It In Dark Current File
Yes
Subtract Dark Current Find Maximum
Display Sealed Data
Plot ?
Yes
Plot Data
No
Find FWHM
Output Maximum, Minimum, & FWHM
6

Figure 25 - continued

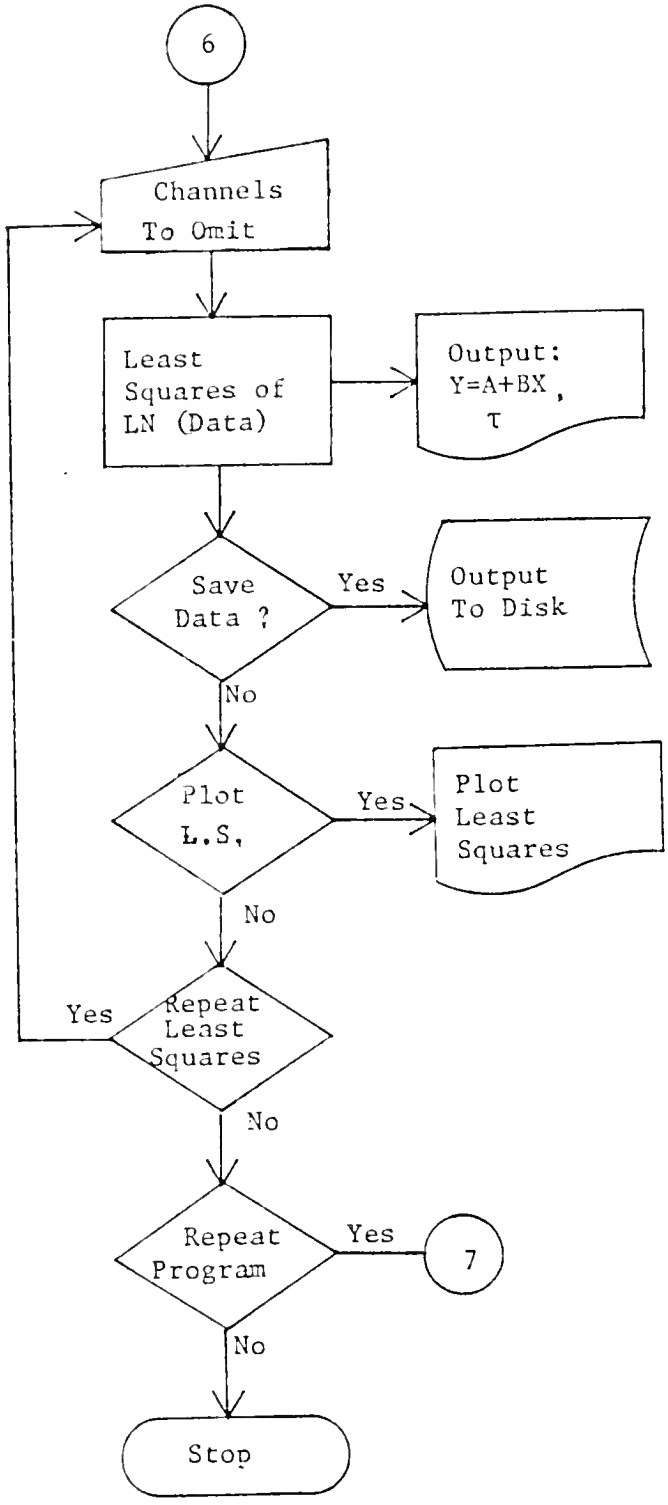
6
Channels To Omit
Least Squares of LN (Data)
Output: Y=A+BX, τ
Save Data ?
Yes
Output To Disk
No
Plot L.S.
Yes
Plot Least Squares
No
Repeat Least Squares
Yes
No
Repeat Program
Yes
7
No
Stop

An important section in the program was to determine how to average the data sets as they were transferred from the TA. Two different routines were written to try and overcome the problems of temporal jitter and drift. These routines were a "peek seek" routine and a "step seek" routine. The peek seek routine found the channel containing the maximum amplitude value for each data set and added the data sets together such that these channels all coincided. A predetermined number of channels (N) could be added together in an attempt to smooth out individual channel-to-channel variations. In this case, the entire data set was broken down into a smaller data set of 256/N points, where each point was made up of a summation of N values from the original data. For this work, with the analysis of laser pulse widths, N = 1 was used.

The step seek routine found the first channel containing an amplitude that was greater than a predetermined threshold value, and added the data sets together such that all of these channels coincided. If the data did not reach the threshold value, new data was transferred and the process repeated.

A third alternative was to simply add the data together, channel-for-channel, as it was transferred. This was the fastest method but offered little signal enhancement.

At the end of the transfer, the FORTRAN program was used to signify an "end of job" to the TA by making one extra data transfer than required for the data analysis. The

assembly language program supplied by Hamamatsu (Appendix D) would not function as desired for this work because the "end of job" handshake control was not included. Also, because of the time involved in using the "peek seek" or "step seek" routines, and because of the TA programming, an "end of job" signal sent to the TA after the data transfer was ignored. Hence, the data transfer subroutine was called again, a dummy set transferred, and an "end of job" sent to the TA immediately thereafter.

After the data transfer, all channels that did not have a value corresponding to the proper number of averages in them were loaded with zeros and the data set was returned to a 256 point array. A dark current subtraction was then performed by using either the dark current file or by finding the minimum data value and subtracting that from each point. From this data set a maximum value was found, the scaled data displayed, and a plot obtained if desired. The maximum and minimum values, as well as a measure of the peak width (FWHM), were printed on the terminal.

The fluorescence lifetime was obtained from a least squares calculation of the natural logarithm of the fluorescence signal versus time information. A single component lifetime was calculated and a deconvolution was not attempted, although the user had to determine what part of the decay curve should be included in the least squares routine. The least squares program could be repeated as many times as desired, the least squares data plotted, or the raw data stored on disk.

APPENDIX D
ASSEMBLY LANGUAGE PROGRAM FOR DATA TRANSFER FROM THE TEMPORAL ANALYZER TO THE DEC PDP 11/34 MINICOMPUTER

The assembly language program TAIN was supplied by Hamamatsu with the Temporal Analyzer for the parallel transfer of data from the TA to the DEC PDP 11 series minicomputers through the DR-11C parallel interface. In Figure 26, the flow chart for this routine is given.

At the entry point of the program, the operating parameters, i.e., data buffer and flag variable, were read in, a "CPU ready" signal sent out, and the flag set to indicate a busy status. An interrupt service routine was enabled to process the data transfer. The service routine stored the data, decremented a counter, and checked to see if all the data was transferred. If not, the subroutine returned to the FORTRAN program, which, in turn, waited for another interrupt. If all the data had been transferred, the busy flag was cleared and the interrupt disabled, then control was transferred back to the FORTRAN program.

The disabling of the interrupt routine was not part of the program obtained from Hamamatsu. It was added because, if another interrupt occurred (as described below) the program would attempt to write data into a fictious data buffer.

Figure 26. Flow Chart for Assembly Language Program Used to Transfer Data from the Temporal Analyzer to the DEC PDP 11/34

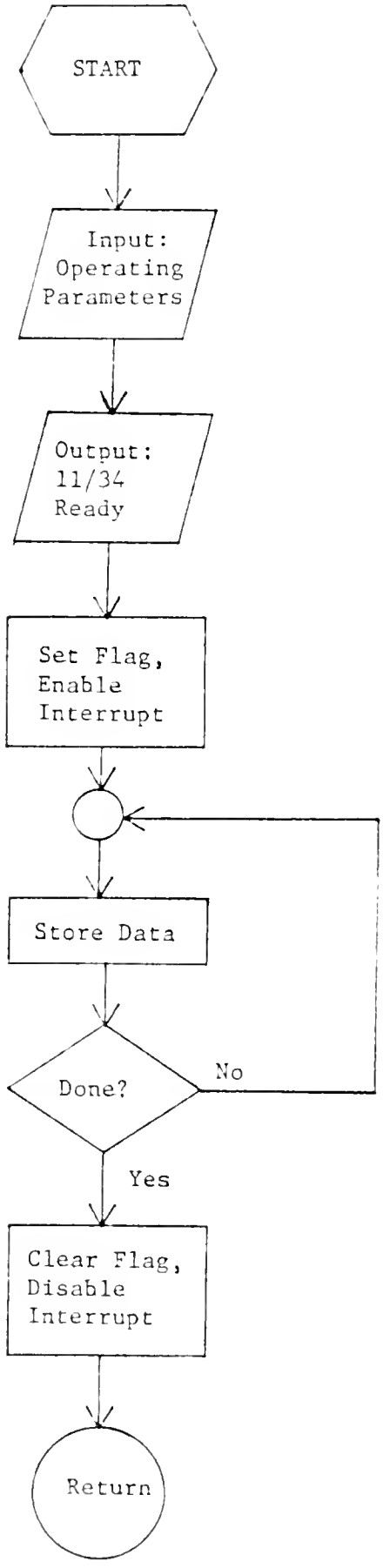
START
Input: Operating Parameters
Output: 11/34 Ready
Set Flag, Enable Interrupt
Store Data
Done?
No
Yes
Clear Flag, Disable Interrupt
Return

There was a minimal amount of "handshaking" required for the transfer of data from the TA to the 11/34. Since the TA was partly hand-wired and partly preprogrammed in read-only-memory (ROM), it was not easily modified. Hence, any changes needed came from the 11/34 end.

With the 11/34 running the FORTRAN program STST, the point was reached where the 11/34 was ready for data transfer and signified this through one of the control lines. The TA was then initialized in the "Fast Transfer" mode. This triggered the pulse generator, which fired the laser and the streak camera. After the streak camera had acquired the temporal information, it triggered the TA which collected the data and began the data transfer. The TA transferred all 256 data points and searched for an "end of job" signal. If and "end of job" was not found, the TA cycled back to the beginning, retriggered the pulse generator, collected more information, and waited for the 11/34 to become ready for the data transfer. In the usual turn of events, the 11/34 was ready before the TA could transfer the information, except after the 11/34 had collected all the data it was programmed to average. It was at this point that the data transfer subroutine had to be called again and an "end of job" sent by the 11/34. The "end of job" signal was sent using the "IPOKE" subroutine from FORTRAN, supplied by DEC.

LIST OF REFERENCES

(1) C.Th.J. Alkemade, W. Snelleman, G.D. Boutilier, B.D. Pollard, J.D. Winefordner, T.L. Chester, and N. Omenetto, Spectrochim. Acta., 33B, 383 (1978)

(2) G.D. Boutilier, B.D. Pollard, J.D. Winefordner, T.L. Chester, and N. Omenetto, Spectrochim. Acta. 33B, 401 (1978)

(3) G.D. Boutilier, J.D. Bradshaw, S.J. Weeks, and J.D Winefordner, Appl. Spectros., 31, 307 (1977)

(4) G.D. Boutilier, Ph.D. Thesis, University of Florida, Gainesville, FL, 1978

(5) Pure and Appl Chem., 45, 99 (1976)

(6) Yu. I. Belyaev, L.M. Ivantson, A.V. Karyakin, Pham Hung Phi, and V.V. Shemet, J. Anal. Chem USSR, 23 855 (1968)

(7) M. Marinkovic and T.J. Vickers, Anal. Chem., 42, 1613 (1970)

(8) C.Th.J. Alkemade, H.P. Hooymayers, P.L. Lijnse, and T.J.M.J. Vierbergen, Spectrochim Acta., 27B, 149 (1972)

(9) J.W. Cooley and J.W. Tukey, Math. Com, 19, 297 (1965)

(10) R.B. Blackman and J.W. Tukey, "The Measurement of Power Spectra", Dover Publications, Inc., New York 1958

(11) J.W. Cooper, "The Minicomputer in the Laboratory", Wiley-Interscience, Inc., New York, 1977

(12) Y. Talmi, R. Crosmun, and N.M. Larson, Anal. Chem., 48, 326 (1976)

(13) G.M. Hieftje and R.I. Bystroff, Spectrochim Acta., 30B, 187 (1975)

(14) W.R. Ware, Transient Luminescence Measurements, Ch. 5, in "Creation and Detection of the Excited State", A.A. Lamola, Ed., Marcel Dekker, New York, 1971, Vol. 1A

(15) J.D. Winefordner, S.G. Schulman, and T.C. O'Haver, "Luminescence Spectrometry in Analytical Chemistry", Wiley-Interscience, New York, 1972

(16) G.G. Guilbault, "Practical Fluorescence, Theory, Methods, and Technique", Marcel Dekker, New York, 1973

(17) J.B. Birks, J. Res. NBS - A. Physics and Chemistry, 80A, 389 (1976)

(18) N. Omenetto, P. Benetti, L.P. Hart, J.D. Winefordner, and C.Th.J. Alkemade, Spectrochim. Acta, 28B, 289 (1973)

(19) J.W. Daily, Appl. Opt. 15, 955 (1976)

(20) D.R. Olivares and G.M. Hieftje, Spectrochim. Acta, 33B, 79 (1978)

(21) P.A. St. John and J.D. Winefordner, Anal. Chem., 39, 500 (1967)

(22) J.D. Winefordner, Acc. Chem. Res., 2, 361 (1969)

(23) R.P. Fisher and J.D. Winefordner, Anal. Chem., 44, 948 (1972)

(24) C.M. O'Donnell, K.F. Harbaugh, R.D. Fisher, and J.D. Winefordner, Anal. Chem., 45, 609 (1973)

(25) K.F. Harbaugh, C.M. O'Donnell, and J.D. Winefordner, Anal. Chem., 45, 381 (1973)

(26) K.F. Harbaugh, C.M. O'Donnell, and J.D. Winefordner, Anal. Chem., 46, 1206 (1974)

(27) T.F. Van Geel and J.D. Winefordner, Anal. Chem., 48, 335 (1976)

(28) M. Zander, Z. Anal. Chem., 226, 251 (1967)

(29) M. Zander, Z. Anal. Chem., 229, 352 (1967)

(30) M. Zander, Z. Anal. Chem., 263, 19 (1973)

(31) G.D. Boutilier and J.D. Winefordner, in press

(32) L.J. Cline Love, L.M. Upton, and A.W. Ritter III, Anal. Chem., 50, 2059 (1978)

(33) L.J. Cline Love and L.A. Shaver, Anal. Chem., 48, 364A, (1976)

(34) J.M. Harris, R.W. Chrisman, F.E. Lytle, and R.S. Tobias, Anal. Chem., 48, 1937 (1976)

(35) W.H. Woodruff and S. Farquharson, Anal. Chem., 50, 1389 (1978)

(36) Y. Onoue, K. Morishige, K. Hiraki, and J. Nishikawa, Anal. Chim. Acta, 106, 67 (1979)

(37) G.D. Boutilier, personal communications

(38) M. Gustavsson, H. Lundberg, and Svanberg, Phys. Lett., 64A, 289 (1971)

(39) R.Z. Bachrach, Rev. Sci. Instrum., 43, 734 (1972)

(40) J.M. Harris and F.E. Lytle, Rev. Sci. Instrum., 48, 1469 (1977)

(41) U.P. Wild, A.R. Holzworth, and H.P. Good, Rev. Sci. Instrum., 48, 1621 (1977)

(42) K.G. Spears, L.E. Cramer, and L.D. Hoffland, Rev. Sci. Instrum., 49, 255 (1978)

(43) K.G. Spears, Laser Focus, 14, 96 (1978)

(44) F.E. Lytle, Anal. Chem., 46, 545A (1974)

(45) F.E. Lytle, Anal. Chem., 46, 817A (1974)

(46) S.I. Green, Laser Focus, 14, 60 (1978)

(47) L.M. Fraser and J.D. Winefordner, Anal. Chem., 44, 1444 (1972)

(48) G. Beck, Rev. Sci. Instrum., 47, 537 (1976)

(49) J.M. Harris, F.E. Lytle, and T.C. McCain, Anal. Chem., 48, 2095 (1976)

(50) V.J. Koester, Anal. Chem., 51, 458 (1979)

(51) J.P. Ryan, Laser Focus, 15, 74 (1979)

(52) J.M. Ramsey, Ph.D. Thesis, Indiana University, Bloomington, IN, 1974

(53) J.M. Ramsey, G.M. Hieftje, and G.R. Haugen, Appl. Optics., 18, 1913 (1979)

(54) Z.D. Popovic and E.R. Menzel, Chem. Phys. Lett., 45, 537 (1977)

(55) E.R. Menzel and Z.D. Popovic, Rev. Sci. Instrum., 49, 39 (1978)

(56) S.L.M. Instruments, Inc., instrument model SLM 4800A, Urbana, IL

(57) H.P. Haar and M. Hauser, Rev. Sci. Instrum., 49, 632 (1978)

(58) G.M. Hieftje, G.R. Haugen, and J.M. Ramsey, Appl. Phys. Lett., 30, 463 (1977)

(59) A. van der Ziel, "Noise in Measurements", Wiley-Interscience, New York, 1976

(60) A. Antic-Janovic, V. Bojovir, and M. Marinkovic, Spectrochim. Acta, 25B, 405 (1970)

(61) V.G. Mossotti, F.N. Abercrombie, and J.A. Eakin, Appl. Spectros., 25, 331 (1971)

(62) G.M. Hieftje, B.E. Holder, A.S. Maddox, and R. Lein, Anal. Chem., 45, 238 (1973)

(63) W.D. Stanley and S.J. Peterson, Byte, 3, 14 (1978)

(64) R.W. Ramirez, Electronics, June 13, 1974

(65) R.W. Ramirez, Electronics, June 26, 1975

(66) Applications notes available from Tektronix, Inc., Beaverton, OR

(67) J.L. Genna, R.M. Barnes, and C.D. Allemand, Anal. Chem., 49, 1450 (1977)

(68) T.G. Mathews and F.E. Lytle, Anal. Chem., 51, 583 (1979)

(69) D.J.S. Birch and R.E. Imnof, Chem. Phys. Lett., 32, 56 (1975)

(70) B. Valeur, Chem. Phys., 30, 85 (1978)

(71) I. Isenberg and R.D. Dyson, Biophys. J., 9, 1337 (1969)

(72) B.R. Hunt, Math. Biosci., 10, 215 (1971)

(73) I. Isenberg, R.D. Dyson, and R. Hanson, Biophys. J., 13, 1090 (1973)

(74) B. Valeur and J. Moirez, J. Chim. Phys. Physiochim. Biol., 70, 500 (1973)

(75) W.R. Ware, L.J. Doemeny, and T.L. Neonzek, J. Phys. Chem., 77, 2038 (1973)

(76) A. Grinvald and J.Z. Steinberg, Anal. Biochem., 59, 583 (1974).

(77) A. Gafni, R.L. Modlin, and L. Brand, Biophys. J., 15, 263 (1975)

(78) A. Grinvald, Anal. Biochem., 75, 260 (1976)

(79) A.E. McKinnon, A.G. Szabo, and R.D. Miller, J. Phys. Chem., 81, 1564 (1977)

(80) G.R. Fleming, C. Lewis, and G. Porter, Chem. Phys. Lett., 31, 33 (1975)

(81) H. Mueller, H. Baessler, and G. Vaubel, Chem. Phys. Lett., 29, 102 (1974)

(82) E.S. Tudron, J.M. Van Prudyssen, and S.D. Colson, J. Chem. Phys., 63, 2086 (1975)

(83) L.V.S. Hood and J.D. Winefordner, Anal. Chem., 38, 1922 (1966)

(84) J.J. Aaron, J.J. Mousa, and J.D. Winefordner, Talanta, 20, 279 (1973)

(85) G.D. Boutilier and C.M. O'Donnell, Anal. Chem., 46, 1508 (1974)

(86) E.Y.L. Bower, Ph.D. Thesis, University of Florida, Gainesville, FL, 1978

(87) E.Y.L. Bower and J.D. Winefordner, Anal. Chim. Acta, 102, 1 (1978)

(88) C.M. O'Donnell and T.N. Solle, Anal. Chem., 48, 175R (1976)

(89) C.M. O'Donnell and T.N. Solle, Anal. Chem., 50, 185R (1978)

(90) A.J. Campillo, V.H. Kellman, and S.L. Shapiro, Science, 193, 227 (1976)

(91) G.R. Fleming, J.M. Morris, and G.W. Robinson, Chem. Phys., 17, 91 (1976)

(92) L. Harris, G. Porter, J.A. Synowiec, C.J. Tredwell, and J. Barber, Biochim, Biophys. Acta, 449, 329 (1976)

(93) Manufacturers literature, Garching Instruments - available through INRAD, Northvale, NJ

(94) I.N. Knyazev, V.S. Letochov, and V.G. Movshev, Opt. Com., 6, 250 (1972)

(95) V.N. Ishchenko, V.N. Listrin, and A.R. Sorokin, Opt. Spectros., 39, 106 (1975)

(96) J.H. Parks, D.R. Rao, and A. Javan, Appl. Phys. Lett., 13, 142 (1968)

(97) G.L. Walden and J.D. Winefordner, Appl. Spectros., 33, 166 (1979)

(98) R.P. Cooney, T. Vo-Dinh, and J.D. Winefordner, Anal. Chim. Acta, 89, 9 (1977)

(99) R.P. Cooney, G.D. Boutilier, and J.D. Winefordner, Anal. Chem., 49, 1048 (1977)

(100) R.P. Cooney and J.D. Winefordner, Anal. Chem., 49, 1057 (1977)

(101) R.P. Cooney, T. Vo-Dinh, G. Walden, and J.D. Winefordner, Anal. Chem., 49, 939 (1977)

(102) Manufacturers literature, Hamamatsu Corp., Middlesex, NJ

(103) D.H. Hartman, Rev. Sci. Instrum., 49, 1130 (1978)

(104) P.F. Jones and A.R. Callow, Rev. Sci. Instrum., 44, 1393 (1973)

(105) Model 162 instruction manual, EG&G, PAR, Princeton, NJ

(106) I. Berlman, "Handbook of Fluorescence Spectra of Aromatic Molecules", Academic Press, New York, 1965

(107) R.S. Becker, "Theory and Interpretation of Fluorescence and Phosphorescence", Wiley-Interscience, New York, 1960

(108) H. Lin and M.R. Topp, Chem. Phys. Lett., 47, 442 (1977)

(109) M.E. Mack, Appl. Phys. Lett., 15, 166 (1969)

(110) M.M. Malley and P.J. Rentzepis, Chem. Phys. Lett., 7, 57 (1970)

(111) C. Lin, T.K. Gastafson, and A. Dienes, Opt. Commun., 8, 210 (1973)

(112) A.N. Rabinov, M.C. Richardson, K. Sala, and A.J. Alcock, Appl. Phys. Lett., 27, 358 (1975)

(113) W.H. Glenn, M.J. Brienza, and A.J. Demaria, Appl. Phys. Lett., 12, 54 (1968)

(114) B.H. Soffer and J.W. Linn, J. Appl. Phys., 39, 5859 (1968)

(115) T.R. Royt, W.L. Faust, L.S. Goldberg, and C.H. Lee, Appl. Phys. Lett., 25, 514 (1974)

(116) L.S. Goldberg and C.A. Moore, Appl. Phys. Lett., 27, 217 (1975)

(117) B. Fan and T.K. Gastafson, Appl. Phys. Lett., 28, 202 (1976)

(118) A.J. Cox and G.W. Scott, Appl. Opt., 18, 532 (1979)

(119) R.J. von Gutfeld, Appl. Phys. Lett., 18, 481 (1971)

(120) C. Lin and C.V. Shank, Appl. Phys. Lett., 26, 389 (1975)

(121) G. Capelle and D. Phillips, Appl. Opts., 9, 517 (1970)

(122) F.P. Schafer, Dye Laser, Springer-Verlag, New York, 1973

(123) R.R. Alfano and S.L. Shapiro, Chem. Phys. Lett., 3, 407 (1971)

(124) E.P. Ippen and C.V. Shank, Physics Today, May, 1978 p. 41

BIOGRAPHICAL SKETCH

Gary Lyle Walden was born in Apalachicola, FL, on August 17, 1951. After attending public schools in Florida, he graduated from Leon High School in Tallahassee. In June 1973, he graduated from Florida State University with a Bachelor of Science in chemistry. He worked for the Indiana State Chemist at Purdue University in West Lafayette, IN, until July 1974 when he accepted a position with the University of Florida, Institute of Food and Agricultural Sciences, in Lake Alfred, FL. In September, 1975, he started graduate studies at the University of Florida. He is a member of Theta Chi Fraternity, American Chemical Society, and the Society for Applied Spectroscopy.

I certify that I have read this study and that in my opinion it conforms to acceptable standards of scholarly presentation and is fully adequate, in scope and quality, as a dissertation for the degree of Doctor of Philosophy.

James D. Winefordner, Chairman
Professor of Chemistry

I certify that I have read this study and that in my opinion it conforms to acceptable standards of scholarly presentation and is fully adequate, in scope and quality, as a dissertation for the degree of Doctor of Philosophy.

Roger G. Bates
Professor of Chemistry

I certify that I have read this study and that in my opinion it conforms to acceptable standards of scholarly presentation and is fully adequate, in scope and quality, as a dissertation for the degree of Doctor of Philosophy.

Robert J. Hanrahan
Professor of Chemistry

I certify that I have read this study and that in my opinion it conforms to acceptable standards of scholarly presentation and is fully adequate, in scope and quality, as a dissertation for the degree of Doctor of Philosophy.

Hugh A. Moye
Professor of Food Science and Human Nutrition

I certify that I have read this study and that in my opinion it conforms to acceptable standards of scholarly presentation and is fully adequate, in scope and quality, as a dissertation for the degree of Doctor of Philosophy.

Martin T. Vala
Professor of Chemistry

This dissertation was submitted to the Graduate Faculty of the Department of Chemistry in the College of Liberal Arts and Sciences and to the Graduate Council, and was accepted as partial fulfillment of the requirements for the degree of Doctor of Philosophy.

December 1979

Dean, Graduate School